

Developing an *In Vivo* Intracellular Neuronal Recording System for Freely Behaving

Small Animals

by

Inho Yoon

Department of Electrical and Computer Engineering
Duke University

Date: _____

Approved:

Bruce R. Donald, Supervisor

Richard Mooney

Gleb Finkelstein

James Morizio

Chris Dwyer

Dissertation submitted in partial fulfillment of
the requirements for the degree of Doctor of Philosophy in the Department of
Electrical and Computer Engineering in the Graduate School
of Duke University

2013

ABSTRACT

Developing an *In Vivo* Intracellular Neuronal Recording System for Freely Behaving

Small Animals

by

Inho Yoon

Department of Electrical and Computer Engineering
Duke University

Date: _____

Approved:

Bruce R. Donald, Supervisor

Richard Mooney

Gleb Finkelstein

James Morizio

Chris Dwyer

An abstract of a dissertation submitted in partial fulfillment of
the requirements for the degree of Doctor of Philosophy in the Department of
Electrical and Computer Engineering in the Graduate School
of Duke University

2013

Copyright by
Inho Yoon
2013

Abstract

Electrophysiological intracellular recordings from freely behaving animals can provide information and insights, which have been speculated or cannot be reached by traditional recordings from confined animals. Intracellular recordings can reveal a neuron's intrinsic properties and their communication with other neurons. Utilizing this technology in an awake and socially behaving brain can bring brain research one step further.

In this dissertation, a customized miniature electronics and microdrive assembly is introduced for intracellular recording from small behaving animals. This solution has realized *in vivo* intracellular recording from freely behaving zebra finches and mice. Also, a new carbon nanotube probe is presented as a surface scanning tip and a neural electrode. With the carbon nanotube probe, intracellular and extracellular neural signals were successfully recorded from mouse brains. Previously, carbon nanotubes have only been used as a coating material on a cell-culturing platform or on a metal based neural electrode. This probe is the first pure carbon nanotube neural electrode without an underlying platform or wire, and it is the first one that has achieved intracellular and extracellular recordings from vertebrate cortical neurons.

Dedication

I dedicate this work to my parent, Jai-Bock Yoon and Cha-Suk Han.

Contents

Abstract	iv
List of Tables	ix
List of Figures	x
Acknowledgements	xiii
1. Introduction	1
1.1 Motivation and scope of dissertation	1
1.2 Relevant background in Neurobiology	3
1.2.1 Neurons and action potentials.....	3
1.2.2 Advantages of intracellular recording.....	4
1.2.3 <i>In vitro</i> and <i>in vivo</i> neuronal recording.....	5
1.2.4 Animal models – mice and zebra finches	7
1.3 Basic properties of carbon nanotubes.....	8
1.4 Contributions of this work	10
2. Developing a customized lightweight microdrive intracellular recording system for <i>in vivo</i> intracellular neuronal recording	13
2.1 <i>In vivo</i> intracellular neuronal recording system.....	13
2.1.1 Pre-existing <i>in vivo</i> intracellular recording systems	13
2.1.2 Development of current <i>in vivo</i> recording rig	14
2.1.3 Anatomy of current <i>in vivo</i> recording rig.....	15
2.2 Developing electric circuits for neuronal recording.....	19

2.2.1	Miniaturizing a headstage.....	20
2.2.2	Test recordings with the mini-headstage.....	23
2.3	Microdrive system.....	24
2.4	Assembly of Yaris.....	27
2.5	Result.....	28
3.	Developing a carbon nanotube based new intracellular electrode.....	30
3.1	Background for neural electrodes.....	30
3.1.1	Glass electrodes and ideal <i>in vivo</i> intracellular electrodes.....	30
3.1.2	Metal or MEMS based neural electrodes.....	32
3.1.3	Carbon based neural electrodes.....	35
3.2	Fabrication of CNT probes as neural electrodes.....	36
3.2.1	CNT fibrils and dielectrophoresis.....	37
3.2.2	Sharpened tungsten tips as dielectrophoresis electrode.....	38
3.2.3	Preparation of CNT solutions and dielectrophoresis parameters.....	40
3.2.4	Annealing of CNT fibril.....	43
3.2.5	Insulation coating.....	44
3.2.6	Focused ion beam cutting.....	45
3.3	Result.....	46
3.3.1	Morphology.....	46
3.3.2	Electrochemical characterization (CV and EIS).....	56
3.3.3	CNT probe as a surface scanning tip.....	60
3.3.4	<i>In vitro</i> intracellular recording.....	62

3.3.5 <i>In vivo</i> extracellular recording	66
3.3.6 Future work.....	69
4. Conclusions.....	70
Appendix A. Anatomy of <i>in vivo</i> intracellular recording setup	72
Appendix B. Mini-headstage PCB layout and its components	73
Appendix C. Connection between the mini-headstage and the commutator	76
Appendix D. Distribution box.....	78
References	81
Biography	89

List of Tables

Table 1: Optimized electrochemical etching parameters.	39
Table 2: CNT solution optimization parameters.	40
Table 3: Components of the mini-headstage.....	74
Table 4: Connection assignment on the mini-headstage.....	75
Table 5: Omnetics connectors and 25 pin D-sub connection assignments.....	77
Table 6: The distribution box (breadboard) connections.....	80

List of Figures

Figure 1: Intracellular recording of passive and active electrical signals in a nerve cell...	4
Figure 2: Visually evoked action potentials and sub-threshold depolarizations.....	5
Figure 3: Schematic drawings of basic intracellular recording setup.....	16
Figure 4: Schematic drawings of <i>in vivo</i> intracellular recording setup.	17
Figure 5: Schematic drawings of current <i>in vivo</i> intracellular recording setup.....	18
Figure 6: A connection diagram for AXOCLAMP™ neuronal recording system for intracellular recording in the current clamp mode.	20
Figure 7: A circuit diagram of the headstage HS-2A-X0.1L.....	21
Figure 8: Modified circuit diagram for the mini-headstage.....	22
Figure 9: The mini-headstage, layout schematic, and allocation of 18 connections.	23
Figure 10: Test recordings with the mini-headstage.....	24
Figure 11: Schematic drawings of zebra finch brain in 45° beak angle	26
Figure 12: CAD drawings of the microdrive chassis and assembly	26
Figure 13: Yaris system with a glass pipette electrode.	27
Figure 14: <i>In vivo</i> intracellular recording with a Yaris system from a freely behaving zebra finch.....	28
Figure 15: <i>In vivo</i> intracellular recording with a Yaris system from a freely behaving mouse with another mouse	29
Figure 16: Metal neural electrodes.....	33
Figure 17: Micro-fabricated neural interfaces	33

Figure 18: Multi-neural electrode for implant	34
Figure 19: CNT probe fabrication flow chart with major process parameters	37
Figure 20: SEM images of a sharpened tungsten tip	39
Figure 21: CNT fibril dielectrophoresis “pulling” stage assembled for this study.....	42
Figure 22: The annealing setup for CNT probe	44
Figure 23: SEM images of SWCNT probe.....	48
Figure 24: SEM images of MWCNT probe.....	48
Figure 25: SEM images of MWCNT probe; (a) near tungsten tip end, (b) texture of MWCNT probe	49
Figure 26: MWCNT probe nodules.....	50
Figure 27: Deformations due to the coating process.....	51
Figure 28: MWCNT probe tip end after the stiffening process	52
Figure 29: MWCNT probe after Parylene coating.....	54
Figure 30: SEM images of a MWCNT probe with 100nm Parylene-C coating.....	55
Figure 31: MWCNT probe tip end after coating Parylene-C and FIB process exposing CNT.....	55
Figure 32: The three-electrode electrochemical cell setup for measuring electrical properties of MWCNT probe	56
Figure 33: Electrochemical characterization of CNT probes.....	58
Figure 34: Nano scale surface profile scan data using a MWCNT probe as its scanning tip	61
Figure 35: <i>In vitro</i> brain slice intracellular recording from mouse, cortical neurons.....	65

Figure 36: <i>In vivo</i> extracellular recordings from mouse brain somatosensory cortex	68
Figure 37: Components of <i>in vivo</i> intracellular recording setup.	72
Figure 38: The mini-headstage PCB layout for each metal layer (projection views).....	73
Figure 39: Components of <i>in vivo</i> intracellular recording setup.	76
Figure 40: The resistor networks with on motor (M _x) for current surge protection.....	79

Acknowledgements

I would like to thank Dr. Bruce R. Donald and Dr. Richard Mooney for letting me join this unique project, and for guiding me through it. I appreciate their generosity and trust in me. This multi-disciplinary project was a very exciting, eye-opening, and valuable learning experience for me in many ways. I am also grateful for Dr. Gleb Finkelstein, Dr. James Morizio and Dr. Chris Dwyer for acting as my dissertation committee members, and providing helpful advice and resources. I also thank Dr. Warren Grill and Dr. Terrence G. Oas for lending me crucial instruments for my experiments, and Dr. Ka C. Wong for his generous help with the FIB at NCSU.

Dr. Ivan V. Borzenets was a great brain storming partner about carbon nanotubes. He was resourceful and generous with testing ideas and discussing early stage experiments.

Dr. Kosuke Hamaguchi was the main collaborator for the neurobiology work in this dissertation. His kindness and relentless research effort has been inspiring, and I hope that outputs of our collaboration will give him a spring board in his career. I must also say thanks to other Mooney Laboratory members (Katie Tschida, Malavika Murugan, Wendy Peh, Jennifer Baltzegar, Anders Nelson, Drew Marticorena, Erin Hisey, Clara Starkweather, David Schneider and Todd Roberts). They embraced me as

an engineer in their great team, helped me on many occasions, and made many fun memorable days.

On a personal note, Dr. Steven Danyluk at Georgia Institute of Technology has been a great supporter. His belief in me has been a solid anchor during windy days. I admire his wisdom and character and hope that I can emulate these traits. Dr. Gregorio Murtagian has been a great friend and I hope we can further develop our unique friendship. I don't have enough words for my parents who have had to wait too long for me.

I express my gratitude to DGS team in Electrical and Computer Engineering department (Autumn Wenner, Dr. Nan Jokerst, Samantha Morton, Dr. Steven Cummer, and Dr. Stacy Tantum). They were very helpful during my difficult days, and went extra miles for my success. I hope they understand that I will not easily forget their help. Finally, I acknowledge partial support from funding sources: Research Incubator Award from the Duke Institute for Brain Science, and NIH grant (NS-79929).

1. Introduction

Study of neural activity in freely behaving animals is an essential step to understand brain function. However, we have a quite limited understanding about how synaptic activity influences sensory perception or the generation of complex behaviors in freely behaving animals. Overcoming technical limitations in current intracellular recording technology can lead to an unparalleled view of individual neurons that will advance our scientific knowledge.

1.1 Motivation and scope of dissertation

Many non-biological tools for neurobiology were invented a few decades ago, and are still very active in the field largely due to the intelligence and well-trained dexterity of the users; however, they could benefit by utilizing the progress of technologies in the last decade to accelerate their research and explore new horizons. We can employ microelectronics, nano materials, and recently developed technologies to overcome old limitations, and help basic science reach the next level.

This study proposes an innovative approach to address a common technical problem with intracellular recording in neurobiology. Current methods are not adequate for long term recording from individual neurons in freely behaving small animals. This limitation is imposed by two technical issues: (i) bulky and relatively heavy electronics

and micro-positioning systems for small animals, and (ii) poor reliability of conventional glass pipette electrodes for chronic recording in freely behaving animals. This study will address both problems.

The overarching goal of this study is developing a new neuronal recording system for *in vivo* intracellular recording from freely behaving small animals. We miniaturized electronics and designed our microdrive system to accomplish the goal without losing compatibility with pre-existing electrophysiology tools and techniques. A new *in vivo* intracellular recording system and successful neural recording from freely behaving animals are introduced in this document.

We also developed a new way to assemble multi-wall carbon nanotubes for a neural electrode. The new technology of making carbon nanotube neural electrodes, and neural recording from them is discussed in chapter 3.

Relevant background of each chapter will be provided at the beginning of the chapter. However, commonly shared neurobiological terms and other conventions are addressed in the first chapter.

1.2 Relevant background in Neurobiology

1.2.1 Neurons and action potentials

The cells of the nervous system can be divided into two broad categories: nerve cells (or neurons), and supporting cells called neuroglia (or simply glia). Among the nerve cells, there is significant diversity in terms of morphology, molecular identity, or physiological activity. Also, the cellular diversity of any nervous system is heterogeneous across species in the size, and shape [1]. The human brain is estimated to contain 100 billion neurons and several times as many supporting cells [2] (A mouse has 75 million neurons [3], and an elephant has 23 billion neurons [2]). Neurons are organized into ensembles or neural circuits processing specific kinds of information instead of working in isolation.

There are three types of neuronal electrical signals: *receptor potentials*, *synaptic potentials*, and *action potentials*. The receptor potentials are due to the activation of sensory neurons responding to external stimuli, and the synaptic potentials are associated with communication between neurons at synaptic contacts. The action potential is an active neuronal response which changes negative transmembrane potential to positive above a threshold potential briefly (about 1 ms). Thus, it is also termed a “spike” or “impulse” and runs down long and rather resistive axons. Action

potentials (APs) are fundamental signals that carry information through the nerve system.

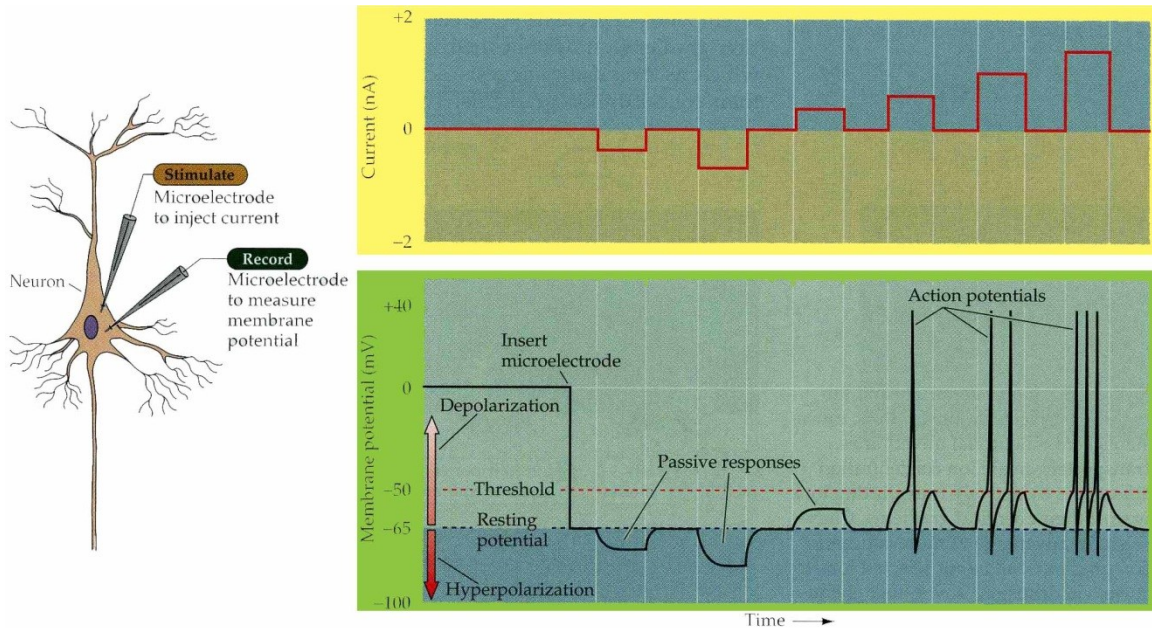


Figure 1: Intracellular recording of passive and active electrical signals in a nerve cell. Hyperpolarizing current pulses produce only passive changes in the membrane potential, while small depolarizing currents also elicit depolarization that cause the membrane potential to meet or exceed threshold additionally evoke action potentials [1].

1.2.2 Advantages of intracellular recording

Details of neuronal activity can be obtained by two types of electrophysiological recordings, extracellular recording and intracellular recording. While extracellular recording offers binary states (*i.e.* APs) of neuronal activity from electrodes placed near the nerve cell, intracellular recording can provide not only the details of action potential

activities, but also smaller, graded synaptic potential changes triggering action potentials with much higher signal to noise ratios. This broader range of information (sub-threshold neuronal activities) from intracellular recordings enables more fundamental studies of underlying cellular and circuit mechanism. [1].

However, studying neural activity in the freely behaving animal has relied on extracellular recording methods due to technical limitations involved in intracellular recording.

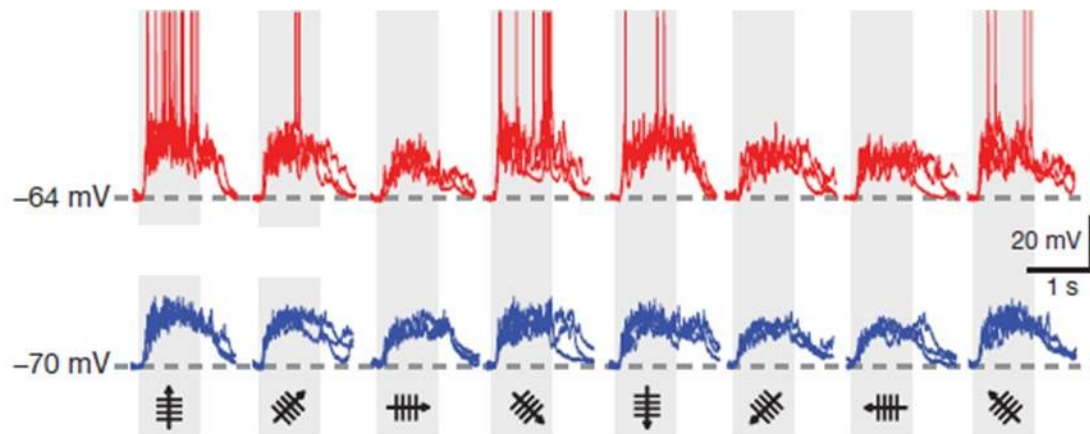


Figure 2: Visually evoked action potentials (upper in red) and sub-threshold depolarizations (lower in blue) responding to drifting gratings of different orientations. If the recording was extracellular, one can interpret that the neuron is responding only to certain angles of visual stimuli [4].

1.2.3 *In vitro* and *in vivo* neuronal recording

Ideally, analyzing neural circuit properties such as neuronal circuit organization, spatial pattern and functional properties of synapses should be based on data collected

directly from freely behaving subjects. However, collecting such data in a behaviorally relevant setting requires miniaturized tools with very high robustness. Because those tools are not commercially available, and custom making them is not a simple task, our current knowledge has heavily relied on data from very restricted settings and extrapolations based from them.

Recording electric neuronal signals from the brain can be acquired from four different settings – *in vitro*, *in vivo* under anesthesia, *in vivo* physically restrained awake animal, and *in vivo* on freely behaving subject. The most limited setting is recording from *in vitro* brain slices prepared after the inevitable sacrifice of the animal. The middle ground between brain slice and freely behaving subject is *in vivo* recording from an anesthetized animal or physically restrained one. One of the most significant disadvantages of the restrained settings is at the complete lack of complex behavior, which is often inseparable for important questions such as brain function of learning from social interactions. Though this middle ground solution is much less technically challenging than using freely behaving subjects, it still shares instability issues arising from the subject's life-supporting functions such as breathing and cardiovascular activities.

Unrestrained animals move abruptly and such movement brings undesirable impacts on recording electrodes and record cells. Even if a cell is captured for a while, an impact on the recording electrode can release the contact. Therefore, it becomes important to get other cells without disturbing the animal or changing the electrode during an *in vivo* recording. Therefore, miniaturization of implantable micropositioning systems has been explored with different actuation methods: manual [5], hydraulic [6], DC servomotors [7], piezo motor [8, 9], synchronous motor [10], vaporization [11], Electro-thermal MEMS [12, 13], and piezoelectric MEMS [14].

1.2.4 Animal models – mice and zebra finches

Animal models have been used in a wide range of research including taxonomic human equivalence, disease models, behavioral sciences, and genetics. This is due to the advantages of animal studies: applicable controls over subjects, ability to withstand invasive measures, speed, uniformity, availability, and cost-effectiveness.

The most commonly used vertebrate model is the mouse (*Mus musculus*). In addition to their fast reproduction rate and availability, they share 99% of their genes with humans. Thus mice make a great model for inherited human diseases, but they cannot be used for a vocal learning study which is important for understanding learning itself and effects of social interaction. Interestingly, neural mechanisms of human speech

learning share strong parallels to complex forms of vocal learning in songbirds [15]. To this end, zebra finches (*Taeniopygia guttata*) are used for studies of the song system and the study of non-mammalian auditory systems. Because of their well-defined learning period and sensitive response to environmental cues, zebra finches are a popular model in neurobiology.

While mice and zebra finches offer great models to conduct important neurobiological studies, their small size becomes a challenging factor for intracellular recording in free awake status. Obviously, only a fraction of their body weight can be put on their heads without disturbing “normal” behavior and zebra finches are much lighter than mice: Freely behaving mice can carry 8.5g on their head [7], but zebra finches can carry only 1.6g [16]. Because intracellular recording requires few essential components near the recording site, reducing the size and weight of essential components becomes a critical issue for intracellular recording in the intact brains of these small animals.

1.3 Basic properties of carbon nanotubes

For long-term, *in vivo*, neural interface applications, a biocompatible electrode should provide biochemical stability, higher charge-injection capacity, and lower impedance with minimal size. It is also required for any neural interface to have proper

mechanical properties such as flexibility, strength, and durability matching its surrounding.

A carbon nanotube's properties depend on its chemical, structural and morphological forms. Electrically, a CNT can be metallic or semiconducting depending on its chirality and number of walls [17, 18]. Strong π -bonds of graphitic structure within each wall make conductivity along the tube axis much superior than across the walls.

Mechanically, single crystal single wall CNT (SWCNT) is the strongest material with Young's modulus greater than 1 TPa [19]. As for Multi-walled CNTs (MWCNT), reported Young's modulus numbers are smaller than SWCNT due to weaker bonding strength between the walls, and higher probability of defects in their structure. However, MWCNT has impressive tensile strength (150 GPa for a 15 nm diameter [17]), 100 times stronger than steel. Due to the high tensile strength, MWCNT can be bent and twisted into a large angle without being broken.

Overall, CNTs have great material properties for neural interface and electrodes; these include low impedance, great mechanical strength, and high surface area to name a few. However, widely favorable CNT assembly for neural applications has not emerged yet. (More background for CNT neural electrodes is discussed in 3.1.3.)

1.4 Contributions of this work

Engineered Devices Enabled Contributions to Neuroscience.

Chapter two of this document is about making miniaturized electronics and a microdrive assembly for *in vivo* intracellular recording from small behaving animals. As described in 1.2.2 and 1.2.3, these neural recordings give unique advantage that cannot be acquired by any other method, and provide great insight of intact brain in a behavioral setting. But achieving that requires customized, miniaturized, and light-weight setup which is compatible with pre-existing techniques and equipment.

We solved this problem by making new custom electronics and microdrives that can capture neurons from zebra finches and mice in an awake and socially behaving status. This allows us to ask and answer more advanced questions in brain studies. For example, Dr. Kosuke Hamaguchi studied auditory-vocal integration, using intracellular recordings in singing finches. He confirmed that the intracellular signal of a cell is very stereotyped to a syllable that a bird sings. He also found that the synaptic activity of HVC_x cells (sub-population of HVC, a sensorimotor nucleus) is insensitive to distorted auditory feedback. These findings contradict previously speculated hypotheses, and provide better understanding of auditory feedback-dependent vocal and dendritic plasticity.

The microdrive assembly is still being used for on-going studies, and some of the *in vivo* recording results have been reported via a conference presentation, which was subsequently been submitted to a journal.

*“Efficient coding of vocal transitions revealed by sparse synaptic activity in the singing bird”,
Society for Neuroscience annual meeting 2012, New Orleans, USA.*

K. Hamaguchi, I. Yoon, B. R. Donald, R. Mooney

*“Mechanisms underlying a synaptic trace of auditory feedback in a sensorimotor nucleus
important to learned birdsong”,*

Kosuke Hamaguchi, Katherine A. Tschida, Inho Yoon, Bruce R. Donald, Richard Mooney

Nanomaterials Designed to Extend Experimental Capabilities in Neurobiology

The third chapter of this dissertation is making CNT into a neural electrode and recording signals from brains. Currently existing neural electrodes have their own limitations, and CNTs have been used to improve existing electrodes. However, previous studies used CNT only as a coating material on a metal wire or a substrate for cultured cells [20, 21]. As explained before, neurons never function in isolation. Therefore, studying isolated, cultured cells is never like working with intact neurons in the brain. Obviously, inventing a new CNT structure or assembly as a direct alternative to conventional neural electrodes (sharp recording electrode or extracellular recording metal wire) is not a simple task, but much more beneficial than previous reports.

This dissertation presents a new way of assembling and using CNTs for neural interface. With our CNT based electrode, we successfully recorded intracellular and extracellular neural signals from mice under *in vitro* and *in vivo* settings. Previously, a simple assembly of CNTs was tested in huge lateral-giant neurons in a crayfish's abdominal ganglion [22]. However, this is the first intracellular recording from relatively small mammalian cortical neurons using a CNT based electrode. Considering the diversity of neurons, validating a CNT based electrode from an important brain area of the most popular animal model (mice) is a significant technological achievement. Therefore, the results presented in this dissertation will provide a solid step for advancing nanomaterials into brain research and broader applications.

The concept of the CNT assembly for neural interface is incorporated into a U.S. Provisional Patent (Application No. 61/711,511), and the work of the CNT probe as a neural interface has also been submitted to a journal.

"Intracellular neural recording with pure carbon nanotube probes"

I. Yoon, K. Hamaguchi, I.V. Borzenets, G. Finkelstein, R. Mooney, B.R. Donald

2. Developing a customized lightweight microdrive intracellular recording system for *in vivo* intracellular neuronal recording

Even though *in vivo* intracellular recording from freely behaving small animals gives great advantages in brain research, only few reports successfully garnered such data. To realize such recording, we decreased size and weight of the custom made headstage and microdrive under 1.3g, so that it will be light enough to be carried by small animals such as zebra finches. Our developments are compatible with conventional glass pipette electrodes and electrophysiology techniques. The headstage and microdrive assembly have been tested for zebra finches and mice, and multiple copies of the assembly are being used for ongoing research.

Given that this study's original contribution is very much integrated into a larger system (*in vivo* recording rig), an integral view of the recording rig is provided before discussing independent contributions. Relevant, but minor details of the system are put in appendix for future reference.

2.1 *In vivo* intracellular neuronal recording system

2.1.1 Pre-existing *in vivo* intracellular recording systems

As mentioned in 1.2.3, *in vivo* intracellular recording can be done under restrained conditions (under anesthesia or a head-fixed configuration). Though these

settings are less ideal than recording from freely behaving animals, it has been shown that intracellular recording can be achieved on head-fixed mice on a spherical treadmill with virtual environments [23].

With a less restrict setting, whole-cell patch intracellular recording has been done (up to 1 hour) with freely moving rats, which are significantly bigger than mice [24, 25]. A custom made headstage, a motor and an electrode were put together for capturing a targeted cell. Then the electrode was fixed on the skull with dental acrylic before releasing the rat.

Even though it is more challenging with smaller animals such as zebra finches and mice, implanting a reliable micro positioning device on subject animals for chronic neuronal recording can improve quality of data and productivity significantly as compared to surgical implantation or manual adjustment of the electrode [10]. With an implanted microdrive assembly, Michael Long *et al.* reported intracellular recording from singing zebra finches [16]. We took this approach, and made our system lighter and more robust than any other reported.

2.1.2 Development of current *in vivo* recording rig

This study inherited an *in vivo* recording rig from John Prather, who assembled the system based on Michael Fee and Anthony Leonard's work [10] and used it for *in*

vivo extracellular recording from singing swamp sparrows and Bengalese finches [26]. The current rig has three major functional groups: commutator, a miniaturized headstage, and a microdrive system. We use the commutator system as inherited, but everything else is a product of this study, with collaboration from Dr. Kosuke Hamaguchi.

2.1.3 Anatomy of current *in vivo* recording rig

The basic function of the rig is passive intracellular recording from a head-fixed animal as shown in Figure 3. Inside of a sound proofing box, the subject animal is at a fixed position with an electrode placed in a targeted brain area. A headstage should be connected directly to the electrode to pass through the neural signal which eventually goes to the recording computer and the Axoclamp. Through the same path, current injection can be delivered to the brain by commending it from the computer via the Axoclamp or directly from the Axoclamp. A speaker for sound stimulation can be placed in the box to deliver controlled sound play from the computer.

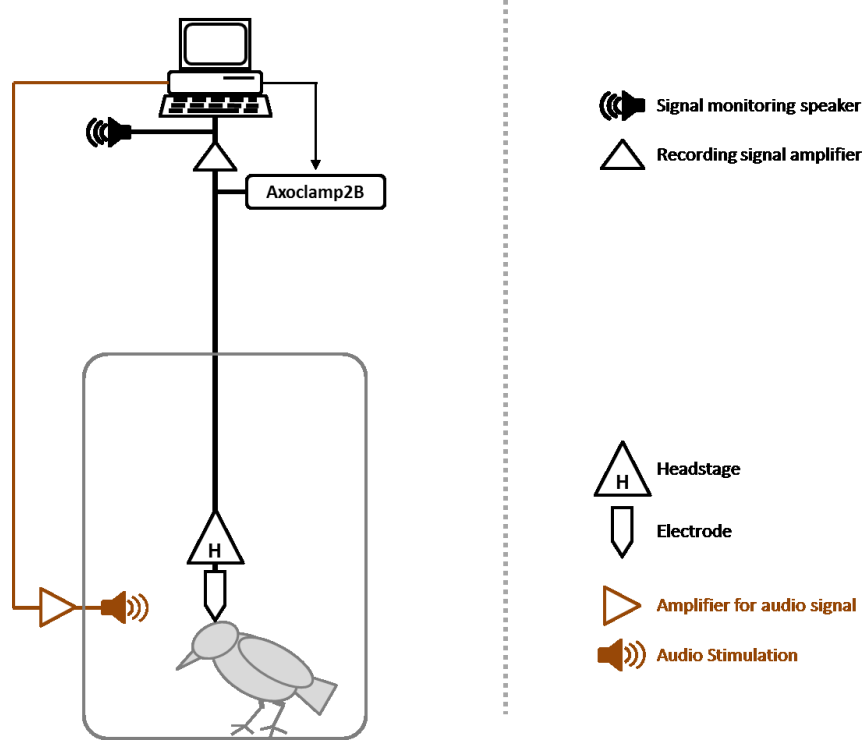


Figure 3: Schematic drawings of basic intracellular recording setup.

To accommodate the freely behaving subject animal, the commutator system (commutator, and red components in Figure 4), a microdrive system, and a miniaturized headstage are added to the basic function of the rig as shown in Figure 4.

The commutator system prevents tangling tethered lines [10]. The headstage had to be miniaturized, and the microdrive system had to be developed to hunt cells without disturbing the animal. After assembling the miniaturized headstage and the microdrive system, the total weight and size should be light and small enough for the subject animals to carry and behave normally. A microphone is placed in the box for sound recording, because an awake and unstrained subject animal can actively respond to

stimuli such as sound and current injection. We can even introduce another animal in the box to provide a social setting.

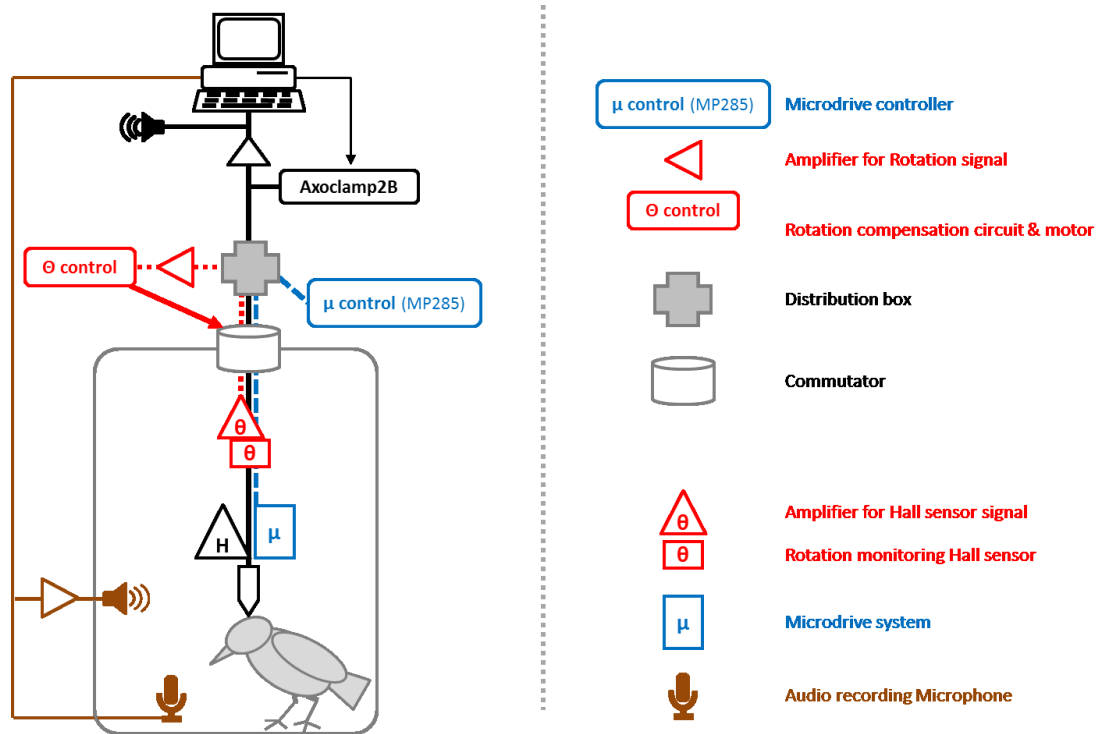


Figure 4: Schematic drawings of *in vivo* intracellular recording setup.

Additionally, we can add separate electrical stimulations via customized mini-headstage (see Figure 5). Video monitoring and video presentation to the subject animal can be accomplished using the same computer also. Another new feature of the current setup is a real-time feedback control using MATLAB xPC Target™ toolbox (developed by Dr. K. Hamaguchi). This addition improves timing control between a stimulus and response, and computing power for real-time feedback (The real-time setup requires a slave computer as shown in Figure 5).

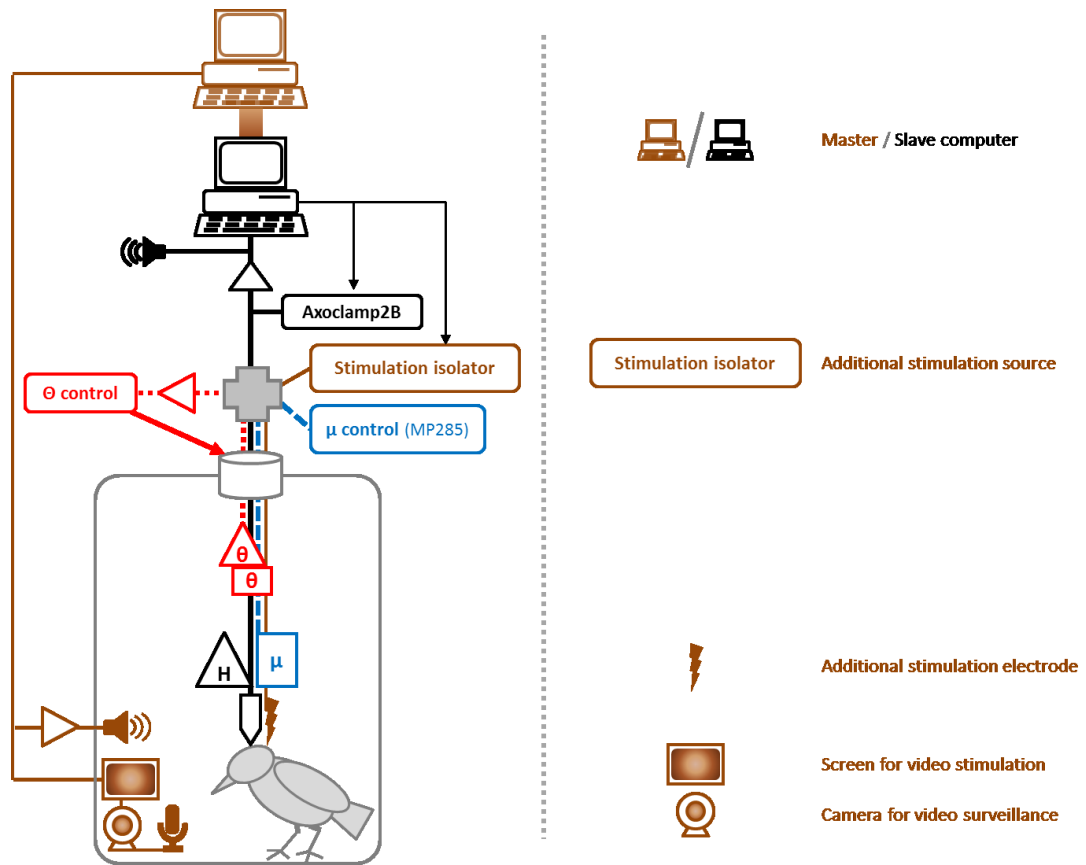


Figure 5: Schematic drawings of current in vivo intracellular recording setup.

In following sections, the miniaturized headstage and the microdrive system will be discussed in more details. Additional materials related to assembly and minor parts of the rig are in the appendix.

2.2 Developing electric circuits for neuronal recording

Although neurons are complex electrochemical systems, they use quick transient voltage, action potentials, for a large portion of their function. Thus electrophysiology uses electronics as its essential experimental tools. For neuronal recording, some portion of the electrical system has to be placed close to the sampling area, and this consumes significantly higher power than what a small size battery can support. This situation demands electronics to be customized for each project, which has become a significant part of neuroscience research in recent years [27-30]. These circuits were primarily designed for *in vivo* extracellular recording or stimulating, typically for larger animals than songbirds. The spectrum of these efforts has a wide range from simple miniaturization on a PCB board to developing a wireless system using microelectronics technology [30, 31].

To be used for freely behaving animals, the whole assembly should be sturdy enough to endure abrupt movements and impacts. It is also important to be aware of the semi-wet interface at the unavoidable exposure of brain surface beneath the skull. Permitting an undesired electrical short circuit on the interface can be disastrous both for the electronics and animal [32].

2.2.1 Miniaturizing a headstage

Developing a whole new electronic system for intracellular recording is not a simple task. In contrast, modifying pre-existing commercial equipment provides benefits of directly inheriting electrophysiological techniques carefully developed over the last decades using the equipment. However, ensuring compatibility of a modified part with a pre-existing setup can be tricky in practice. For our study, we decided to modify only the terminal electronic component, a headstage. The electronic system used in this study is a commercial product from Axon Instruments, Inc. (now Molecular Devices, Sunnyvale, CA USA)).

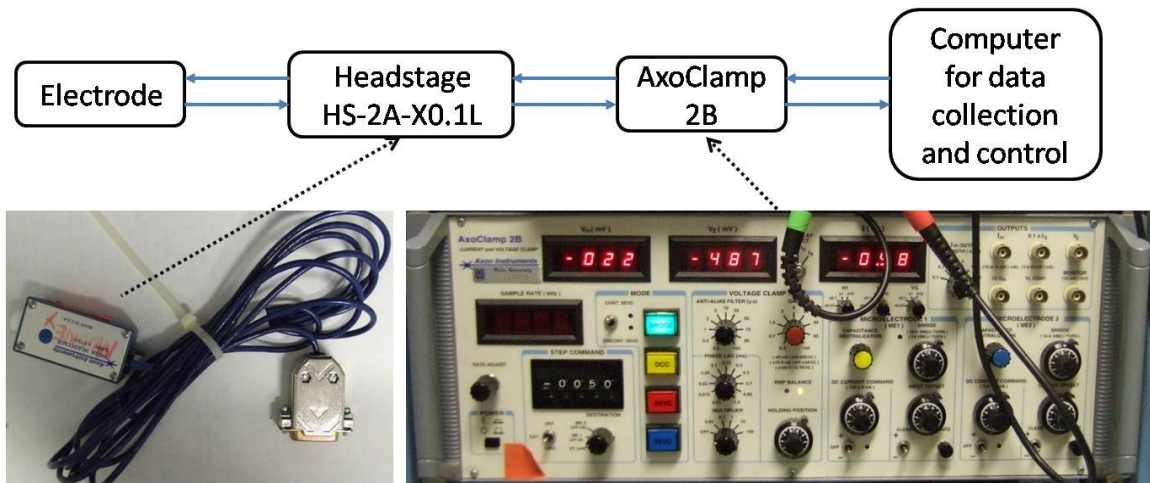


Figure 6: A connection diagram for AXOCLAMP™ neuronal recording system for intracellular recording in the current clamp mode.

In the context of intracellular recording (current clamp mode), the headstage serves two purposes, as a pathway for the injection current and as a voltage follower [33]. Due to the weakness of neuronal signals, the headstage – at least some part of it –

has to be placed right next to the sampling site. Therefore, miniaturizing the headstage became an essential task for the project.

The AxoClamp drives five functions, current injection, signal amplification, bridge balance, capacitance compensation, and “buzzing”. The buzzing is a brief, high-frequency oscillatory current injection through the electrode. Therefore, any modification of the headstage circuit should be compatible with the AxoClamp functions.

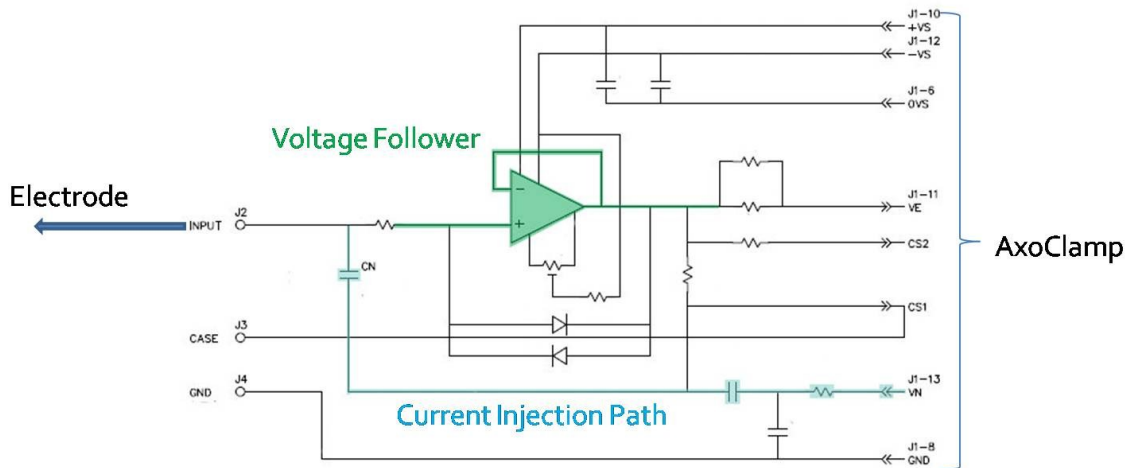


Figure 7: A circuit diagram of the headstage HS-2A-X0.1L

I designed a customized headstage (mini-headstage) to substitute for the commercial headstage (HS-2A-X0.1L, Axon Instrument Inc.). The targeted weight was less than 0.5 g with a minimalistic footprint (less than 10×15 mm²). 4 layer FR4 PCB with thickness of 0.02 inch was chosen for cost, and minimal trace and pitch of connecting

lines on PCB was 0.007 and 0.0025 inches respectively. The PCB was made via Advanced Circuits (Aurora, CO USA), and I assembled it with off-the-shelf components. The assembled customized circuit is called the mini-headstage for the rest of this document.

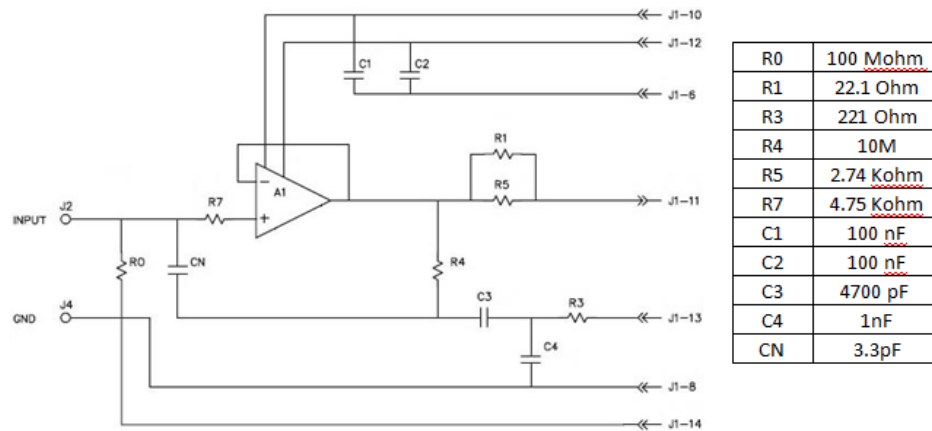


Figure 8: Modified circuit diagram for the mini-headstage.

The main component of headstage is the operational amplifier (op-amp). The original headstage used OPA103 (BURR-BROWN), a low drift – low bias current FET op-amp. We used OPA627 (BURR-BROWN), Difet® op-amp for the mini-headstage. Both op-amps have low input bias current (10 pA max for OPA 627, and 1 pA max for OPA103) and significantly higher output-voltage ($> \pm 5$ V) than interested neuronal potential range ($< \pm 100$ mV). The new op-amp has low corner frequency for Flicker noise ($F_c = 100$ Hz) and provides better low-noise quality (5.6 nV/ $\sqrt{\text{Hz}}$ ($f = 1\text{kHz}$) and 4.8 nV/ $\sqrt{\text{Hz}}$ ($f = 10\text{kHz}$) for OPA627, as opposed to 30 nV/ $\sqrt{\text{Hz}}$ ($f = 1\text{kHz}$) and 25 nV/ $\sqrt{\text{Hz}}$ ($f = 10\text{kHz}$) for OPA103).

As shown in Figure 9, the mini-headstage also serves as an essential electrical connection hub for *in vivo* intracellular recording. The final size of the mini-headstage is 8.5×11 mm and its weight is only 0.4 g which meets the requirements pretty well.

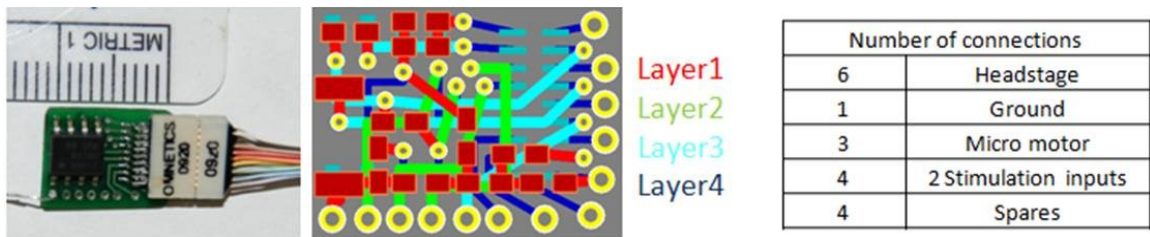


Figure 9: The mini-headstage, layout schematic, and allocation of 18 connections.

After finishing the component assembly, a protective coating is applied on the mini-headstage to prevent particle or moisture contamination near subject animals. Five μm Parylene-C protective coating was applied on the mini-headstage by Chemical Vapor Deposition (CVD) with masks on electrical connection areas.

2.2.2 Test recordings with the mini-headstage

To ensure full compatibility with the AxoClamp, we tested the mini-headstage in multiple settings (Figure 10). After passing the first test using a model cell – an electrical circuit mimicking living cells, the mini-headstage was tested with conventional glass micropipettes on mouse brain slices. Transverse brain slices were prepared from a

mouse (~ 30 days post natal) for the test. We successfully recorded intracellular neuronal signals from neurons in layer II / III (Cerebral cortex) and there was no difference in the headstage functions and signal qualities compared to the commercial headstage.

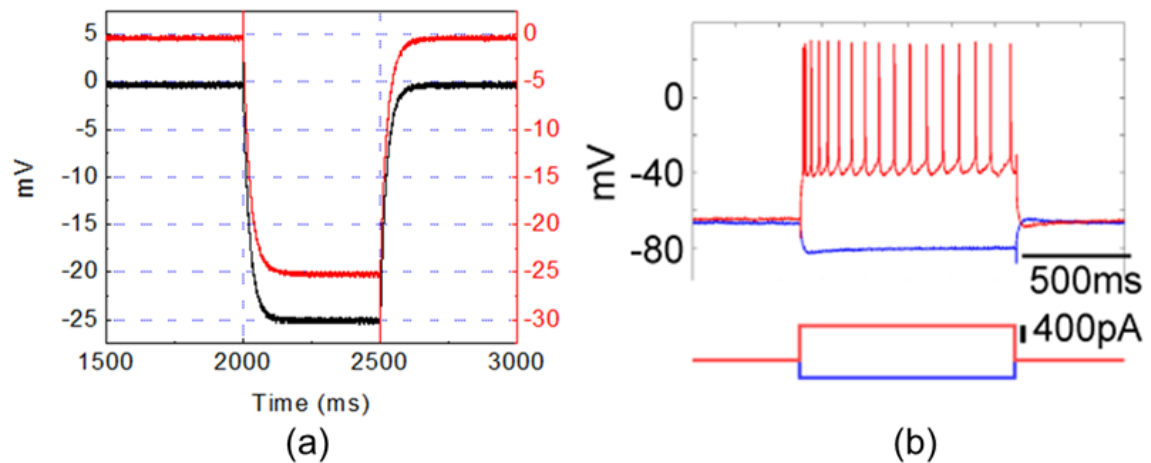


Figure 10: Test recordings with the mini-headstage. (a) Current clamp recordings (-500 pA for 500 ms) obtained using a model cell. The black voltage trace was obtained with the original Axon headstage and the red trace with the miniaturized headstage; traces have been offset by 5 mV for comparison. (b) An *in vitro* intracellular recording made from a layer II/III cortical neuron in an acute brain slice using the miniature headstage (*top*, voltage trace; *bottom*, injected current).

2.3 Microdrive system

Major design constraints for a microdrive systems that drive intracellular recording electrodes in freely behaving small animals are weight, foot print size compared to the skull, range of movement (a few mm), resolution of movement in μm

range, and tolerance against a semi-wet environment on the brain surface. Among few possible directions meeting the constraints, we choose to develop our microdrive from earlier system of M. Fee and colleagues [10, 16]. Our microdrive is primarily designed for zebra finches. However, the same system can also be used for mice, because mice have a larger skull and can carry more weight.

Our microdrive system has a DC motor, a shuttle, a glass electrode, and the chassis holding all of them (see Figure 12). The micro brushless DC motor (Part # 0206A001B+02/1 47:1-Y2825) is made by Faulhaber (Micromo, Clearwater, FL), and its rotating axis is a threaded rod, fitting the shuttle. A custom made shuttle joins the motor and recording electrode and translates the rotation of the motor axis into a linear motion of the electrode. The recording electrode was prepared in the same way as sharp intracellular recording electrodes, and the blunt side of the electrode got cut to a proper length (close to the length of the chassis). The chassis is made by stereolithography (Agile Manufacturing, Inc., Ontario, Canada) from our CAD design, and a typical material choice for the stereolithography was ACURA55. The chassis design gets modified to custom fit a specific need or for better position adjustment.

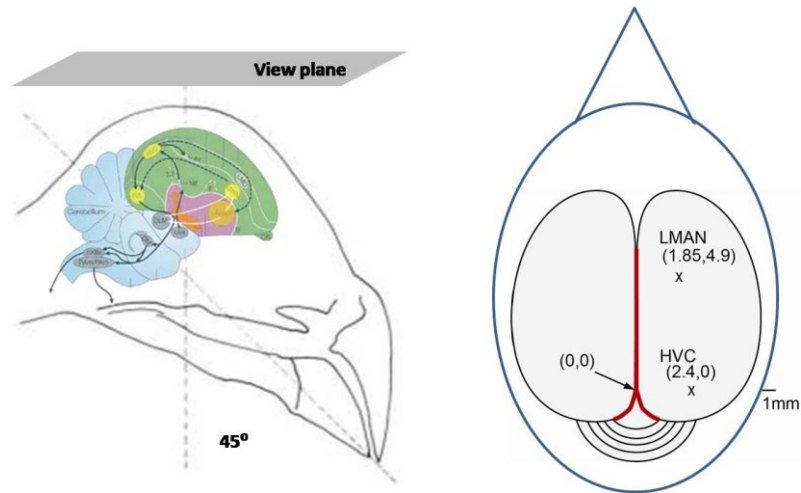


Figure 11: Schematic drawings of zebra finch brain in 45° beak angle (a stereotaxic position, left, modified from [34, 35]); relative coordinates of areas of interested in the view plane (in mm, right).

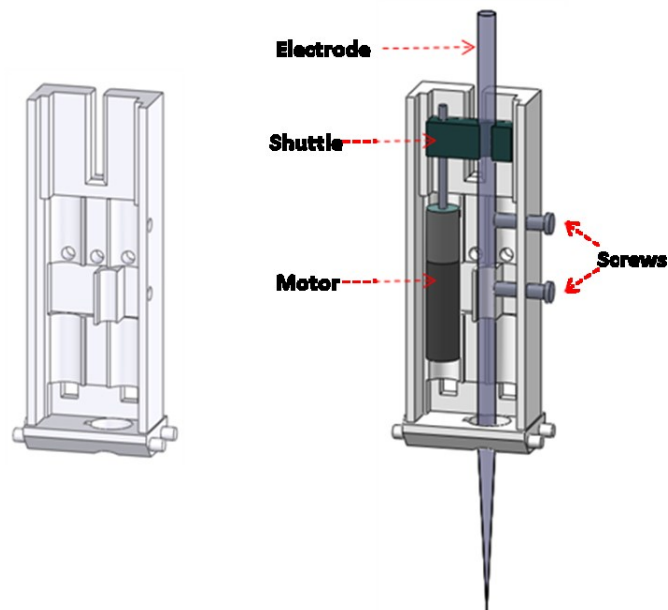


Figure 12: CAD drawings of the microdrive chassis and assembly. (Size of the chassis is $\sim 7 \times 4.5 \times 20 \text{ mm}^3$)

The motor controller is a MP-285 with a FEE modification board (Sutter Instrument, Novato, CA). The motor driving commend were sent via three electric lines via mini-headstage.

2.4 Assembly of Yaris

After we confirmed the compatibility with pre-existing equipment, we integrated the mini-headstage with the microdrive, and the whole assembly is named Yaris (Yari; a spear in Japanese). A basic Yaris assembly weighs 1.2 g, which is lighter than previously reported (1.6g in [16]), and zebra finches could sing in 2 days after implant surgery.

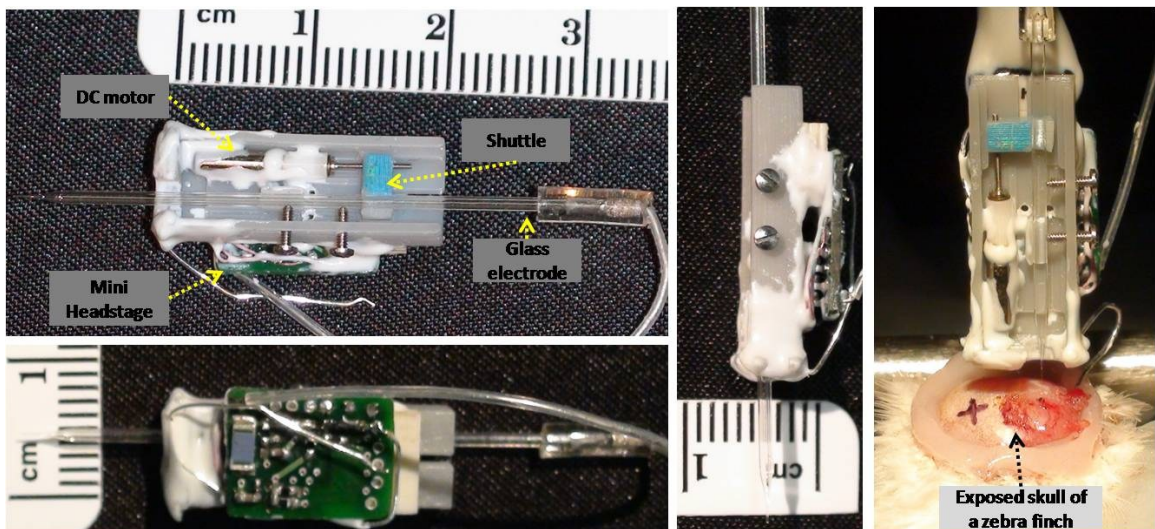


Figure 13: Yaris system (microdrive + the mini-headstage) with a glass pipette electrode.

To prevent EM noise and particle contamination on the assembly, a Faraday shield is put on the whole assembly. The shield is made out of copper plated conductive

fabric (thickness 0.006 inch, surface resistivity $\leq 0.1 \Omega/\square$, Less EMF Inc, Lantham, NY).

The shield size is slightly larger than the Yaris assembly, so that it can fit the Yaris without pressing any component.

2.5 Result



Figure 14: *In vivo* intracellular recording with a Yaris system (microdrive + the mini-headstage) from a freely behaving zebra finch. Left: video monitoring via an inside camera; the bird is pecking a seed tray. Right: real-time intracellular signal on an oscilloscop

With the Yaris system, intracellular neuronal recording has been collected from freely behaving zebra finches to address questions that cannot be addressed with constrained songbirds. The system is compatible with pre-existing intracellular setups and techniques (such as buzzing and current injection). The baseline of the membrane

potential was stable once a captured cell was stabilized as shown in Figure 14. For some extreme cases, a cell could be monitored over several hours while the subject zebra finch was awake and active.

The recordings have been presented at conferences and submitted to a journal. Further experiments with this system are currently ongoing with zebra finches and mice. We believe this technique will be used for many years to fully investigate this new modality of study.



Figure 15: *In vivo* intracellular recording with a Yaris system (microdrive + the mini-headstage) from a freely behaving mouse with another mouse. Left: video monitoring via inside camera, left mouse is the subject. Right: real-time intracellular signal (lower green trace).

3. Developing a carbon nanotube based new intracellular electrode

Conventional intracellular recording technology has been developed with glass micropipettes (glass electrodes) over past decades. Therefore, most of the electrophysiology equipment and techniques have been optimized to work with glass electrodes for a long time. However, glass electrodes still lack a few key properties desired for an ideal intracellular neuronal electrode such as mechanical toughness and higher electrical conductivity. Improvement of these properties could enable intracellular recording methods in challenging environments, including long term recordings in freely behaving animals. With those interests in mind, we developed a CNT based neural electrode (CNT probe). We have acquired intracellular recordings in mice brain slices and in the intact brain of anesthetized mice with the CNT probe.

3.1 Background for neural electrodes

3.1.1 Glass electrodes and ideal *in vivo* intracellular electrodes

Two types of glass micropipettes have been heavily used for neuronal recordings: “sharp” electrode with high impedance ($>100\text{ M}\Omega$, $<50\text{ nm}$ tip radius) and whole cell “patch” electrodes with lower impedance ($1\text{-}20\text{ M}\Omega$, $\sim 1\text{ }\mu\text{m}$ diameter) [33, 36]. The sharp electrode tip is better for delicate penetration without inducing massive

depolarization and leakage of cytosol. However, the sharp tip readily breaks during normal brain movement and introduces many movement-related artifacts due to its large impedance. In contrast, the patch pipette has advantages in signal quality but results in rapid exchange of the pipette solution with the cytosol, therefore disrupting the cell's biochemical equilibrium. This process of dialysis, which also occurs with sharp electrodes, can severely alter neuronal excitability. Finally, the extremely rigid and blunt tip of the patch pipette is poorly suited to recording in the moving brain. Beyond the limitations, both types of glass micropipettes present more challenges especially for intracellular recordings in a freely behaving animal. These issues are mechanical, biochemical and electrical in nature.

An ideal intracellular electrode in a freely behaving animal demands challenging properties such as high conductivity and toughness with flexibility. It is challenging because the requirements ask for sets of material properties which typically do not get along: flexibility with excellent durability in the small scale, very low impedance (*in vivo* resistance less than $M\Omega$) yet having nano-scale tip radius ($< 100\text{nm}$). In addition to those contradicting requirements, it also must be corrosion resistant without evoking undesirable immune responses or any bio-fouling such as unstable protein build-ups.

3.1.2 Metal or MEMS based neural electrodes

Three correlated aspects should be considered when developing neuronal electrodes: (a) electrode materials, (b) fabrication techniques, and (c) biocompatibility. Basic understanding about how different materials interact with the *in vivo* environment has been obtained by studying metals and semiconductors with various metal coatings for neuronal recording [37-43]. It has been found that their electrical performance is significantly affected by the electrical double layer at the interface between conductor and electrolyte.

As for metals, the relatively simple fabrication techniques enabled their use in many pioneering studies [44]. Platinum, iridium, platinum-iridium, gold, stainless steel, tungsten, and molybdenum have been used as core materials; and quartz glass, Teflon, polyimide and Parylene are materials used for insulation via a range of adopted techniques from micromachining to semiconductor manufacturing technologies [45]. More recently, a high aspect ratio tungsten electrode was made by Focused Ion Beam (FIB) machining [46]. Although metal electrodes are still used in neuronal recordings, they are limited in their minimum size and design flexibility compared to semiconductor based electrodes.

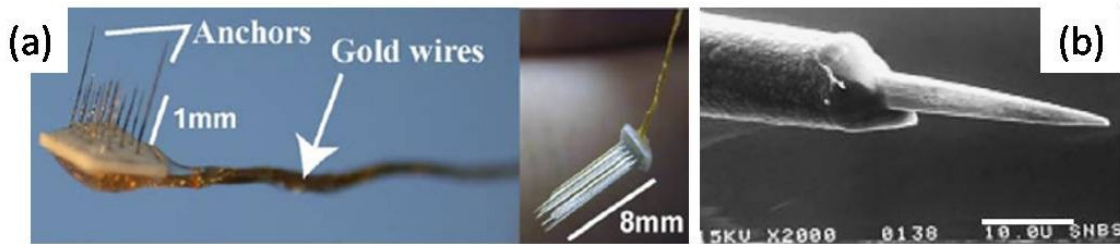


Figure 16: Metal neural electrodes. (a) Metal based electrodes arrays, (b) SEM of an electrode (platinum/iridium with Parylene-C coating) [47].

Benefiting from current microfabrication techniques, semiconductor based electrodes provide the potential of high accuracy, repeatability, and the ability to integrate signal processing circuits with micro actuators.

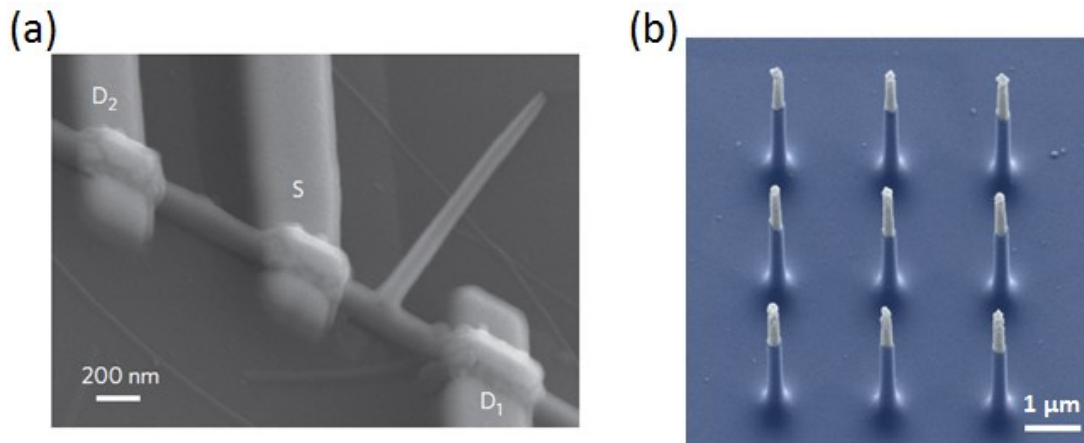


Figure 17: Micro-fabricated neural interfaces. (a) A field-effect transistor for recording action potentials [48], (b) Vertical electrode arrays for culturing a neuron and recording from it [49].

Another benefit of semiconductor wafer based electrodes is its ease of designing multiple recording sites within an array. The well-known silicon based many electrode

arrays (MEA) are the Michigan and Utah probes [50, 51]. On the downside, fragile semiconductor based electrodes can cause significant damage in the brain during insertion. Additionally, stiffness of electrical connections and the out-of-substrate morphology make further integration of electronics and/or actuators on the shared substrate very difficult.

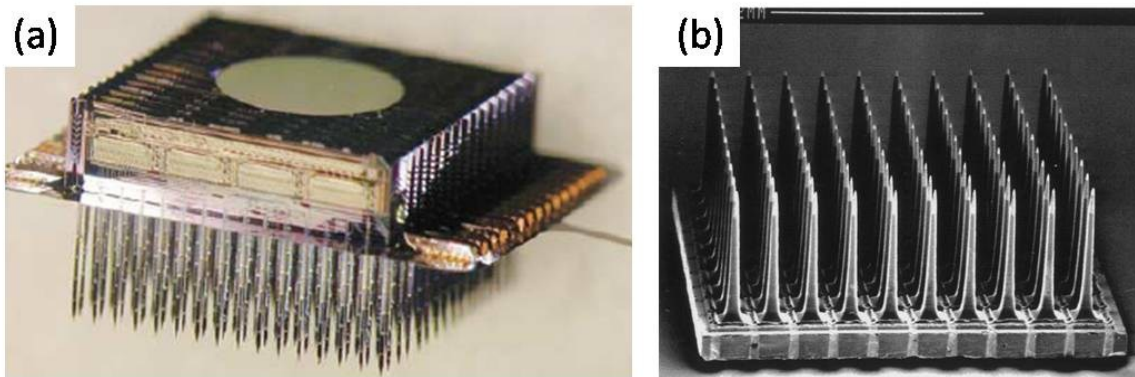


Figure 18: Multi-neural electrode for implant. (a) 1024-site 128-channel neuroelectronic interface [51], and (b) the Utah array (the scale bar above the image is 2 mm) [50].

Although the large number of well-defined multisite recording electrodes have their benefits, most of these new electrodes are developed for extracellular recording, and are simply not suitable for *in vivo* intracellular recording on small, freely behaving animals.

3.1.3 Carbon based neural electrodes

Carbon Nano Tubes (CNTs) are biocompatible, and have even been used in neuroscience applications by fabricating patterned CNTs on SiO₂ substrates to control the growth of cultured neurons [52-55] and covalent attachment of neurotrophin to carbon nanotubes [56]. CNTs also satisfy the contradicting mechanical properties of Atomic Force Microscope (AFM) tips by restoring to their original straight shape from buckling as stress is alleviated. With nano-scale diameter and verified low resistance (typically in K Ω range), CNTs are extremely attractive candidates for use as intracellular recording electrodes [22, 57].

Integrating a CNT as a neuronal electrode has been approached from several angles, but four major approaches will be discussed in this section. The simplest approach is applying CNT as a coating layer on a metal wire [20]. Previous research has shown that the CNT coating improves recording quality. However, using CNT just as a coating layer does not fully exploit great mechanical properties of CNTs, and blunt tip end of the coated electrode cannot be used for intracellular recording.

The second approach, maybe the most straight forward one in terms of assembling concept, is attaching a CNT onto the cantilever of an atomic force microscope (AFM) or onto a similar MEMS platform. However, these CNT electrodes

still suffer from poor yield, weak mechanical junctions, fragileness and limited shape of AFM tips [21, 58].

The next one is making carbon nanopipettes using classical glass pipettes. The process is essentially the deposition and growth of carbon materials inside of pre-pulled and catalyst deposited glass pipettes, followed by selective glass tip etching [59]. These electrodes exhibited recovering from buckling, but effective resistance was too high ($10^9 \Omega$ range).

Last, assembling CNTs at a sharpened metal tip using an electric field and a CNT dispersed solution was tried [60]. Compared to attachment on AFM tips, attachment of CNT was more stable in the aqueous environment and much easier to assemble. Measured resistivity was $\sim 10^6 \Omega$. We adopted this technology for making a neural electrode.

3.2 Fabrication of CNT probes as neural electrodes

Figure 19 is a flow chart of the fabrication process of the CNT probe, and each fabrication process is discussed in the following sections.

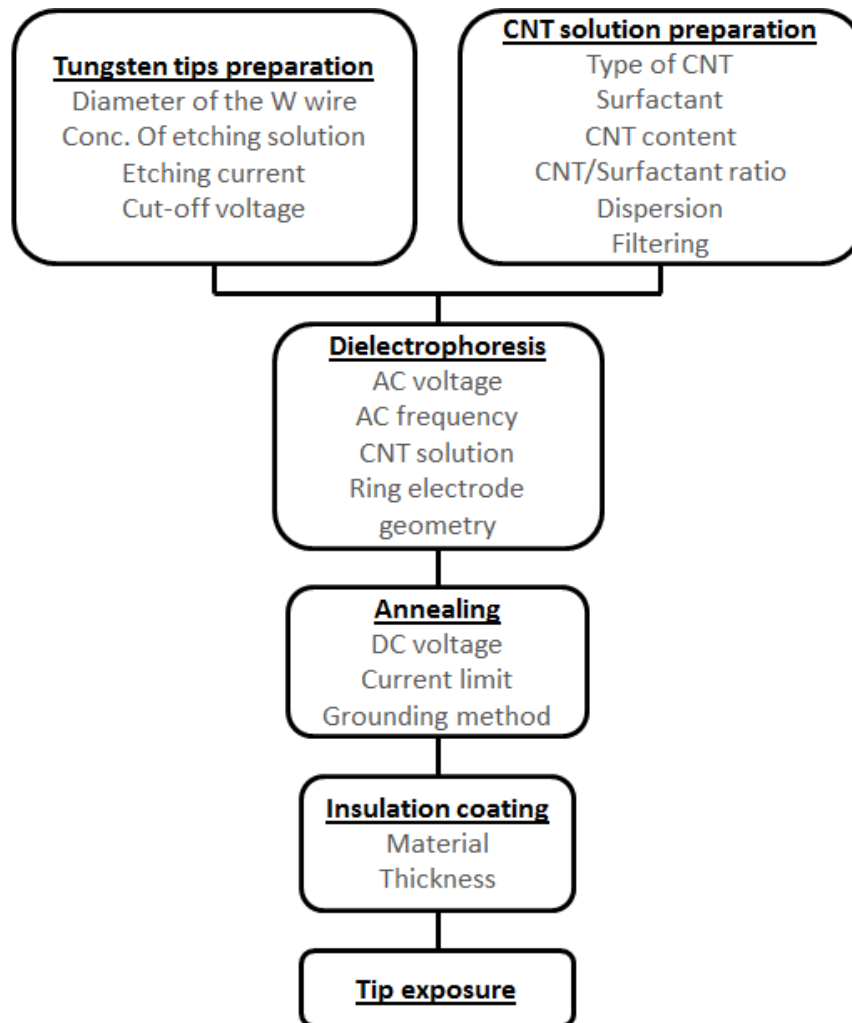


Figure 19: CNT probe fabrication flow chart with major process parameters.

3.2.1 CNT fibrils and dielectrophoresis

Dielectrophoresis uses a non-uniform electric field to affect μm sized particles in a medium. It is independent from polarity of the electric field, but dielectric particles are attracted to the stronger electric field. Prior to our study, this phenomenon was adopted

to make CNT fibrils using CNT dispersed solutions as media [61, 62]. In those reports, there were several interesting observations, particularly for our applications: (a) the technique works for single-wall CNT (SWCNT) and multi-wall CNT (MWCNT), (b) it can generate long and homogeneous thin fibrils (over 1 cm in length, 30-50 nm in diameter with SWCNT), (c) short fibrils (< 50 μm) are relatively stiff, and (d) long fibrils are flexible and can bend sharply without fracture. Because of these characteristics and CNT's material properties, this is an ideal combination for a neural electrode. Therefore, we adopted dielectrophoresis to make CNT fibrils and evaluate them as intracellular neuronal electrodes.

3.2.2 Sharpened tungsten tips as dielectrophoresis electrode

As mentioned in the previous section, dielectrophoresis makes particles, CNTs in our case, to gather at a stronger electric field region. Hence previous studies used a ring type electrode placed just below the level of the solution and a sharpened counter electrode to collect CNTs as a fibril from the center of the ring by gradually pulling the tip away from the solution surface. Since the sharpness of the tip will dominate the intensity of the electric field, the sharpness of the electrode is an important parameter for reproducibility.

Required sharpness of the electrode can be achieved by mechanical pulling of the wire, pulling Indium tip out of its melt, or electrochemical etching of a metal wire. Considering later handling of the fibril and reproducibility, we chose electrochemically etching tungsten wire for this study.

Tungsten is often etched in Sodium-Hydroxide or Potassium-Hydroxide solution (1-6 molar concentration) under applied AC or DC field (10-100 mA current). An electrical cutoff circuit is also needed in order to achieve sharp tips [63]. We optimized the etching parameters (Table 1) for a high aspect ratio with good reproducibility as shown in Figure 20.

Table 1: Optimized electrochemical etching parameters.

Electrochemical etching parameters	
Wire	Tungsten 0.123 mm (diameter)
Etching Solution	NaOH, 4N
Current limit	15 mA
Cut off voltage	12.7 V

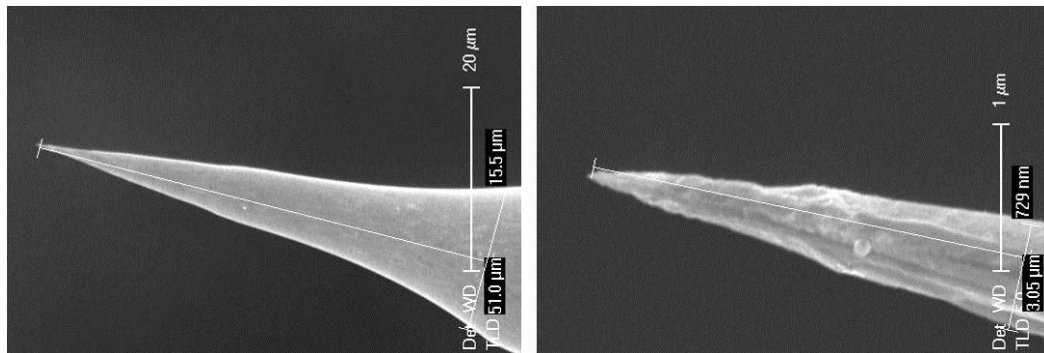


Figure 20: SEM images of a sharpened tungsten tip by the optimized electrochemical etching process (in different scales).

3.2.3 Preparation of CNT solutions and dielectrophoresis parameters

The sharpness of the tungsten tips, the concentration of the CNT solution, the drawing rate, and the electrical field gradient and frequency are reported as controlling parameters for probe morphology [61, 62]. We confirmed those claims through our early parametric experiments for our dielectrophoresis process optimization. However, we learned that dispersion of CNTs is the most critical above all the other dielectrophoresis parameters.

Table 2: CNT solution optimization parameters.

CNT	MWCNTs (95w%, 8-15 nm O.D.)
	SWCNTs (90w%, 1-2 nm O.D.)
Surfactant	PVP (Polyvinylpyrrolidone)
CNT content / 100 mL DIW	0.25 - 0.5 g
PVP/CNT weight ratio	10 - 30 %
Sonication	A probe type, High power cycle 2 - 14 min
Centrifuge	1000 - 4000 RPM, 5-30 min

Types of CNT, mixing ratio, sonication process, and centrifuging had to be adjusted for the right combination. Our CNTs (MWCNTs (95 wt%, 8-15 nm O.D.) and SWCNTs (90 wt%, 1-2 nm O.D.)) were purchased from Cheap Tubes Inc. (Brattleboro, VT, USA). Following suggestion from the manufacturer, Polyvinylpyrrolidone (PVP) was used as a surfactant and a mixing ratio of CNT solution was determined after a few optimization processes (Table 2). High power sonication with a proper cooling cycle is

critical for the dispersion, and centrifuging was essential for removing agglomerated particles and impurities.

My current recipe for the CNT solution is as follows:

- i) CNT 0.4 g, Polyvinylpyrrolidone (PVP) 0.12 g, Deionized Water (DIW) 40 mL.
- ii) A high-intensity ultrasonic processor, Misonix Sonicator 3000, is used to promote dispersion ($[(30 \text{ sec maximum amplitude} + 10 \text{ sec break}) \times 4] \times 10$, effective time is 20 min in total).
- iii) Centrifuge with 3000 RPM, for 20 min. Then discard the precipitate.

The recipe is optimized primarily for MWCNTs (SWCNTs must be dispersed more gently, using lower power and longer time for sonication). I also observed that the solution obtained with this protocol can maintain dispersion stability for over a month. However, I found out that the shelf time of CNT (before mixing) affects dispersion significantly. The best dispersion was obtained when a fresh batch of MWCNT got dispersed within a couple of days after its arrival. The optimally dispersed solution was the least viscous, and the solution made an easily reversible separation after one day. This separation left relatively clear water in the top part of the container. However, the separation did not have any agglomerated bigger particles at the bottom, and it was easy to reverse by simply shaking. A month later, the same solution preparation process with one-month-old CNTs could not produce the same dispersion characteristics such as viscosity and precipitation.

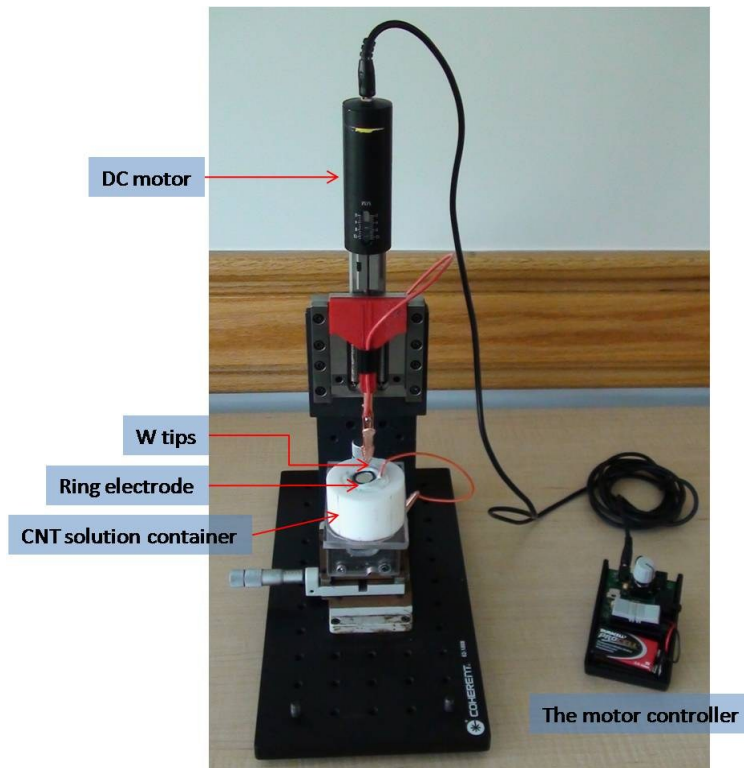


Figure 21: CNT fibril dielectrophoresis "pulling" stage assembled for this study.

We assembled a dielectrophoresis "pulling" stage with a DC motor as shown in Figure 21. Various size ring type electrodes (diameter 4 - 25 mm) were made out of an electrical connection wire (24 AWG). The applied AC field between the tungsten tip and the ring electrode were typically 2 ~20 MHz sinusoidal with 5~80 V peak to peak amplitude. The latest parameters we used for MWCNT dielectrophoresis are;

- i) 25 mm diameter ring type electrode

- ii) 10 MHz sinusoidal potential field with 60 or 80 V peak to peak amplitude (Frequency synthesizer (PTS D310RHo2x-6/x-54) + Amplifier (Amplifier Research 25A250AM6)).
- iii) Pulling speed was kept minimal (40 $\mu\text{m}/\text{sec}$) at the beginning, and gradually increased to maximum toward the end for termination.

3.2.4 Annealing of CNT fibril

Usually, the CNT fibrils made from the dielectrophoresis process are not stiff enough to survive the following insulation coating process, which exposes the CNT fibrils to turbulent gas flux in a Chemical Vapor Deposition (CVD) vacuum chamber. The turbulence is strong enough to deform the samples; typically, very fine tip end with a few CNT could not survive the coating process without becoming tangled in itself.

While testing DC dielectric breakdown for burning off the tip-end (which will be discussed subsequently), I found out that the process made the CNT probe stiffer. So, the process is used before the insulation coating to prevent irreversible deformation of the CNT probes during the coating process.

First, the end of the probe is placed near the gold plated glass surface (Figure 22 (a)) or on top of a DI water droplet (Figure 22(b)) with a micro stage (similar to Figure

21), while proximity of the tip end is monitored with an optical microscope. The “stiffening” process uses increasing DC voltage, up to a threshold value which ranges 80V to 400V, with a limited current (1 or 100 M Ω with a DC power source, Power Design 2K20 (max 20mA)). When a threshold voltage was reached, there was an abrupt and very brief moment when the tip sparks and burns off the end of the probe (on a rigid surface) or almost immediate cutting off a bit of the probe (< 10 μm) generating tiny water mist nearby (on DI water droplet).

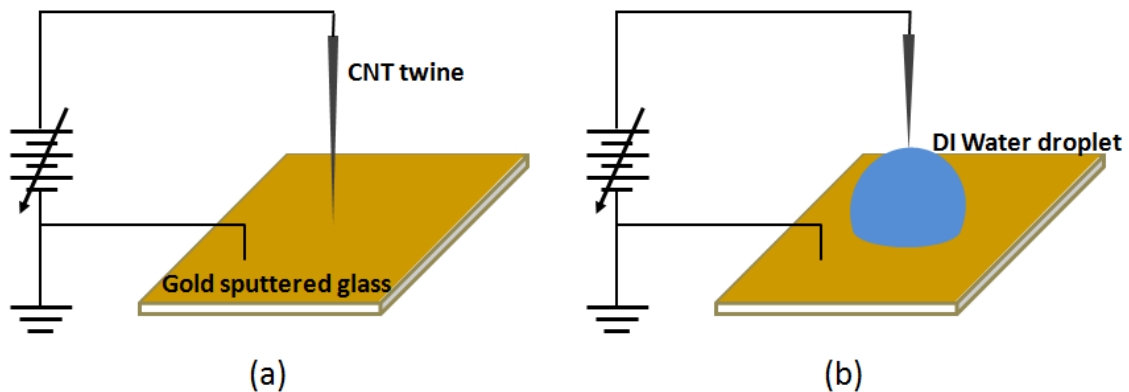


Figure 22: The annealing setup for CNT probe. Adjustable DC power supply posing high voltage on CNT probe against (a) grounded gold sputtered glass, or (b) grounded DI water droplet.

3.2.5 Insulation coating

Because CNT probe is conductive everywhere, bio-compatible electrical insulation must be applied except at the tip end. Parylene-C is biocompatible and also

known to be a good insulating material for recording neuronal activity over long periods [64]. Therefore, we chose it for the coating material in this study. The Parylene coating process is usually done by LPCVD (Low-Pressure Chemical Vapor Deposition), which makes a uniform coating within the chamber. We have applied 200 ~ 300 nm thickness Parylene-C coating on CNT probes. Because the coating system is making a conformal coating on any exposed surface inside of its vacuum chamber, the coating at the very end of the CNT probe has to be removed after the coating for a controlled electrical contact area.

3.2.6 Focused ion beam cutting

Considering that the average cell body of smaller neurons is around 10 μm in diameter, the insulation-free part of CNT probe tip should be significantly less than 10 μm in diameter. To achieve that goal, we tried several approaches. We started from cutting the probe with a surgical knife and scissors which was not successful. Then we moved on to RIE (Reactive Ion Etching) with silicon wafer masking. Granted that we have not put too much time into this method, our experiment revealed that the masking method is not very effective in controlling the extent of burning off, and it is not easy to find the appropriate process parameters. After these initial attempts, we settled with two

methods for exposing the ends; DC dielectric break down to burn off the end, and FIB (focused ion beam) to trim the end with great control.

Dielectric breakdown setup is exactly identical to the annealing process shown in Figure 22 (a) with similar process parameters. This process literally burns off the end part of the probe leaving a relatively blunt end without Parylene-C. As for FIB, we used FEI Quanta 200 3D FEG at the Analytical Instrumentation Facility at NCSU. Ga⁺ beam was accelerated to 30 kV and its current was 1 nA for rough cutting and 100 pA for final trimming. The cylinder like morphology of the CNT probe shaped into a wedge shape similar to the tip of a flat head screwdriver.

3.3 Result

3.3.1 Morphology

3.3.1.1 SWCNT probe vs. MWCNT probe

The parameters of the dielectrophoresis were optimized for yielding 1 to 2 mm length of pure CNT structures with a tapering end. Typically, the diameters of the probe were homogeneous (2-8 μm) and termination and tapering toward the end was achieved by increasing pulling speed. With the ranges of parameters mentioned in the previous

sections, we could make mm scale CNT probes with SWCNT (Figure 23) and MWCNT (Figure 24).

The SWCNT probes were thinner, smoother, and significantly less stiff compared to MWCNT probes. Though the first two qualities are great for the applications of the study, the mechanical quality of the structure was a significant disadvantage. The SWCNT probe was flexing greater than 90 degrees with weak air flow in a lab, and it was clear that it would not survive further handling even after stiffening and more parameter optimization. Thus, we concentrated our effort with MWCNT. MWCNT probes were stiffer than the SWCNT probes, but they have protruding MWCNTs (< 200 nm) on the side wall as shown in Figure 24.

Morphology of MWCNTs on tungsten wire is like ivy on walls as shown in Figure 25 (a), and body of probe had densely self-entangled MWCNT throughout (Figure 25 (b)). However, tapering could be made so that there is only one or few MWCNT at the tip.

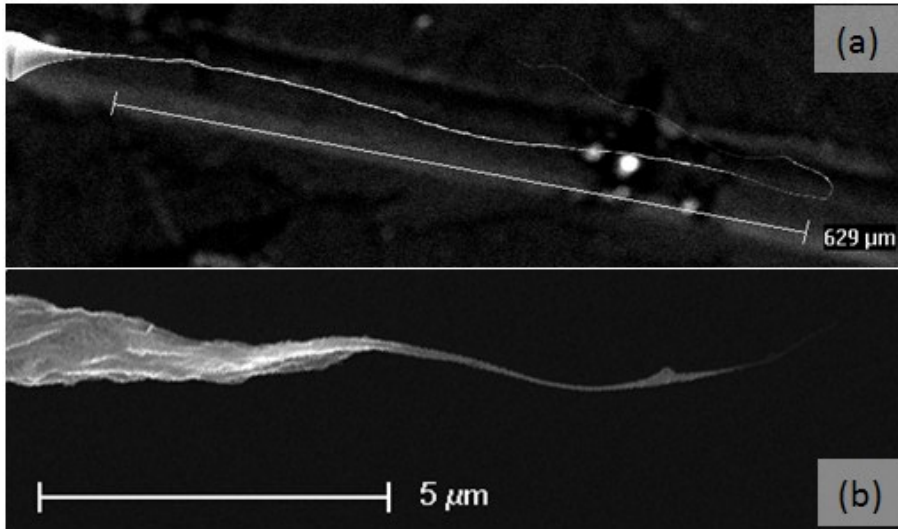


Figure 23: SEM images of SWCNT probe.

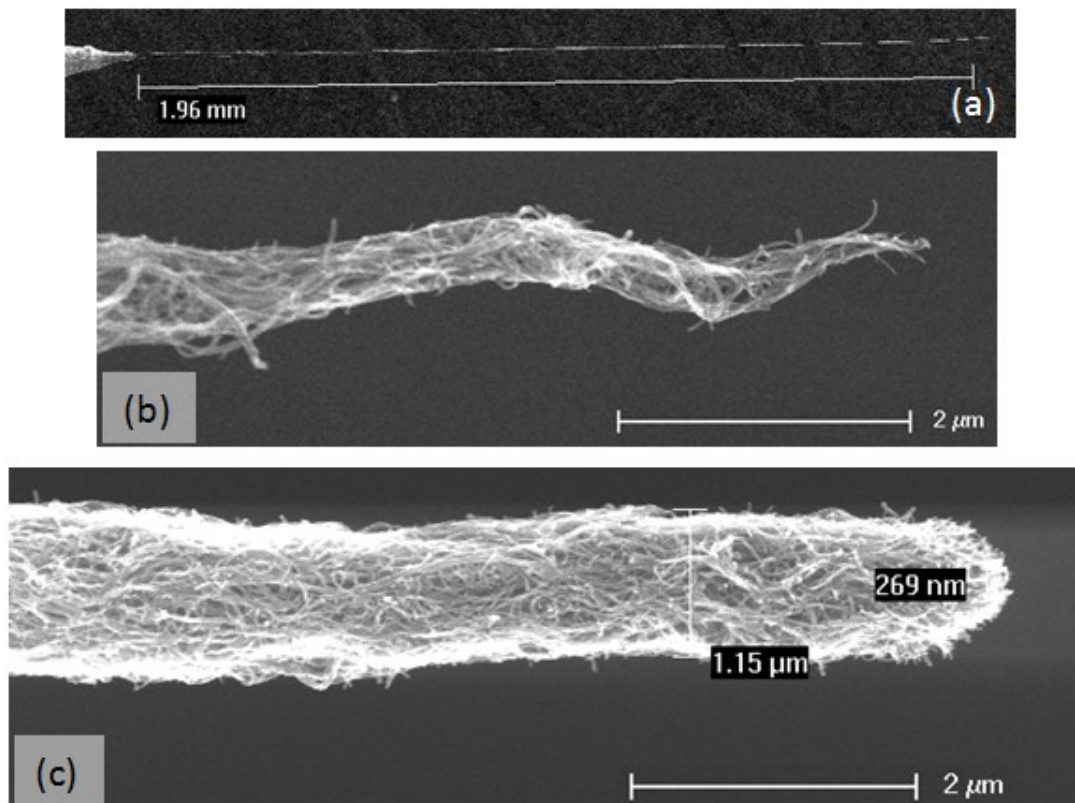


Figure 24: SEM images of MWCNT probe.

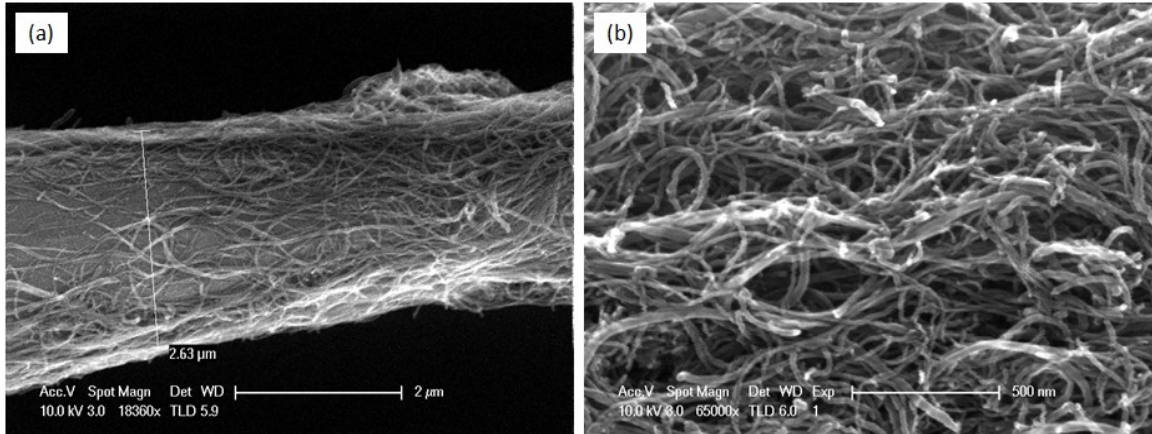


Figure 25: SEM images of MWCNT probe; (a) near tungsten tip end, (b) texture of MWCNT probe (the scale bar is 500 nm).

3.3.1.2 Nodules and tangling

As mentioned in 3.2.3, the dispersion quality of CNTs in solution affects the morphology of CNT probes most significantly. The sonication of the CNT solution and the shelf life of the CNTs themselves are the key parameters for the viscosity and dispersion stability of the solution, the smoothness of the side walls, and the diameter of the CNT probe. Nodules in the probe (shown in Figure 26) are also due to insufficient sonication and extended shelf life of CNTs before mixing.

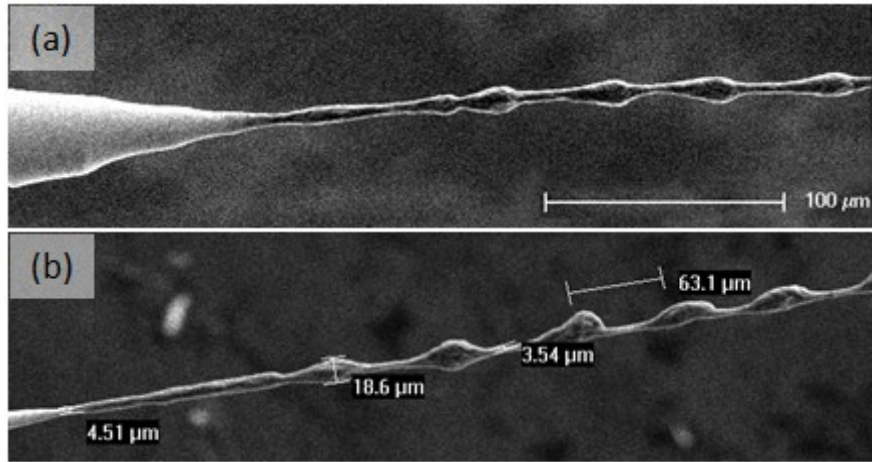


Figure 26: MWCNT probe nodules.

The Parylene-C coating process often makes CNT probes to bend (Figure 27 (d)), or tangle as shown (Figure 27 (a-c)). Placing CNT probes in the middle of the coating chamber space with pointing them downward was the best configuration for mitigating this low yield process. However, the yield of the process was still only 5% without annealing before the coating.

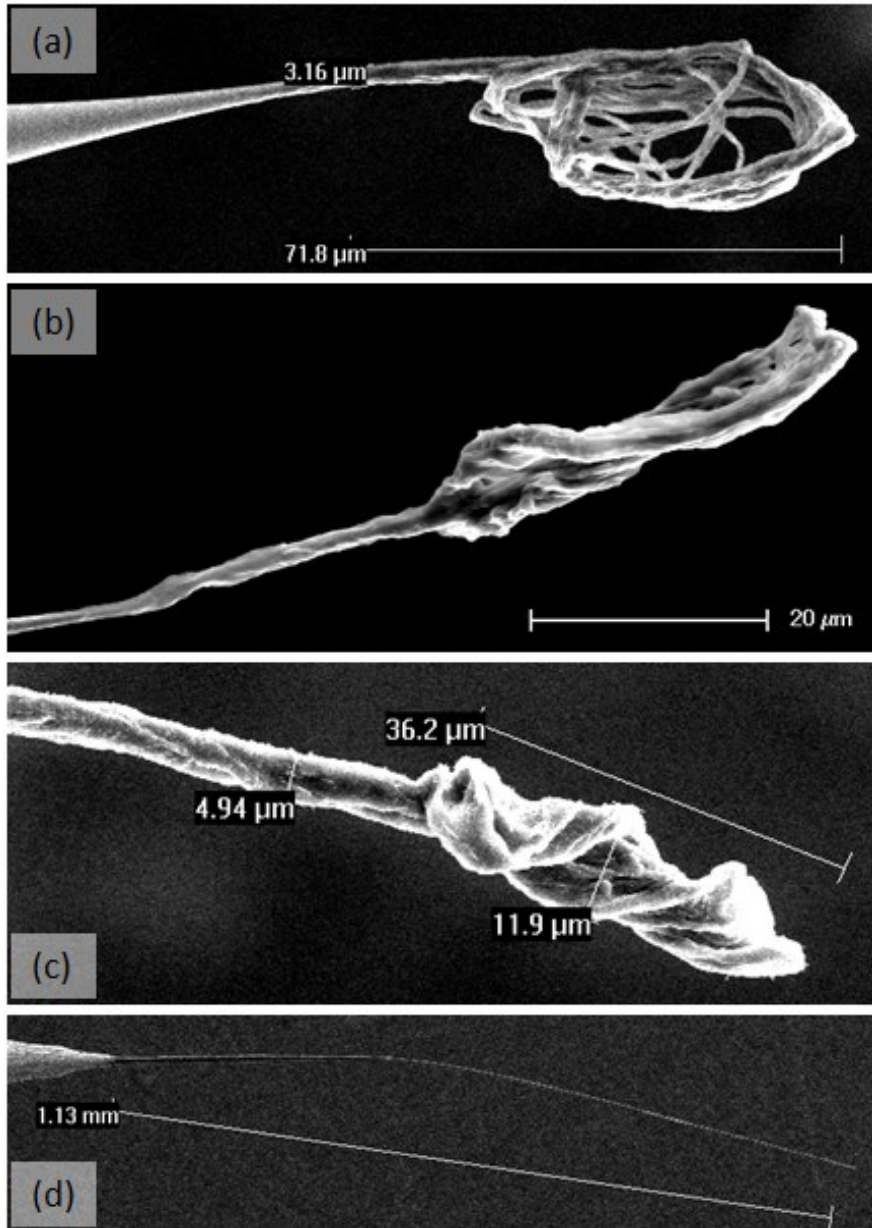


Figure 27: Deformations due to the coating process. (a) and (b) tangled SWCNT probe, (c) tangled MWCNT probe, (d) bent MWCNT probe.

3.3.1.3 Annealing (Stiffening)

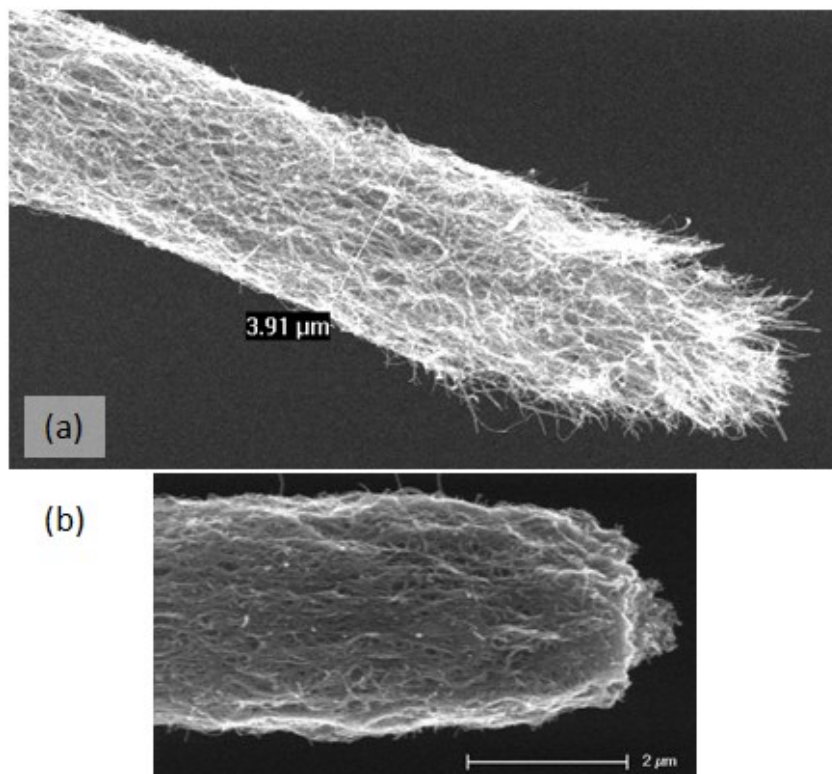


Figure 28: MWCNT probe tip end after the stiffening process (a) with conductive glass surface, (b) with DI water droplet.

Annealing (stiffening) is done by DC dielectric breakdown. When it is done against a gold coated glass surface, the tip end morphology produced sticking out CNTs as shown in Figure 28 (a). Even with limited current (100 MΩ in the line) for the breakdown process, the resulting shape was not suitable for making a smooth, conformal Parylene-C coating and for penetration into cells. The same process on a

grounded DI water droplet gave much more control for the process with less volatility; when the breakdown happens on a gold coated glass surface, it usually burns up a few tens of μm with tiny flame that you can see under the microscope. In all cases, the process can also straighten the CNT probes along the path of shortest distance between the tungsten tip end and the grounded surface.

I suspect that the mechanism of this stiffening is annealing of the CNTs as the current passes through the contact points of CNTs within the probe. However, conductivity measurement of the CNT probe in 0.25 M PBS solution against an Ag/AgCl palette did not show any significant change, except that annealed samples had better stability with the measurement. An obvious disadvantage of this process is sacrificing the sharp end of the probe; however, the yield of following Parylene-C coating process gets significant improvement with the stiffening process, less than 5% to 80%.

3.3.1.4 Insulation coating and tip exposure

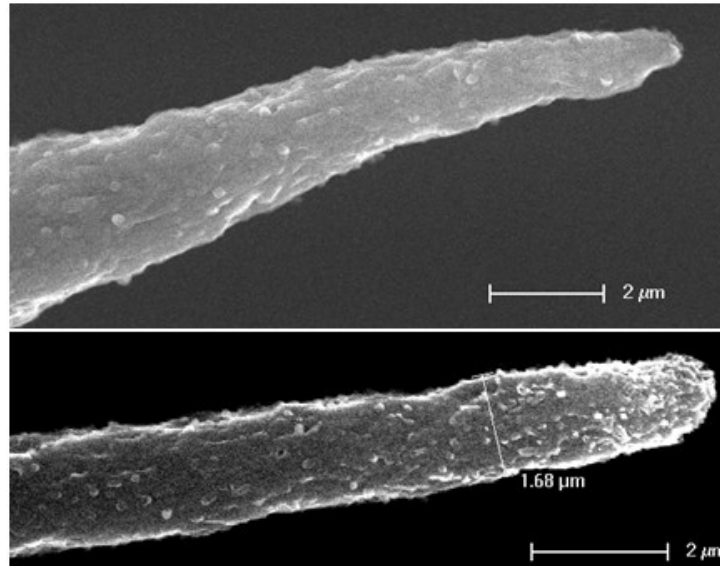


Figure 29: MWCNT probe after parylene coating.

The Parylene-C coating was conformal all around the CNT probe as shown in Figure 29. The coating thickness had to be between 200nm or 300nm to cover the protruding CNTs on the side walls. As mentioned in section 3.2.6, DC dielectric breakdown and FIB were used to expose the probe end to make it electrically conductive. DC dielectric break down removed a few μm of Parylene-C coating from the terminated end (Figure 30). However, the more problematic issue was the shape of the end. With this relatively blunt end, we could not impale any neurons during an *in vitro* brain slice test. However, we could see some shadow of neural activities, which we believe were extracellular signals.

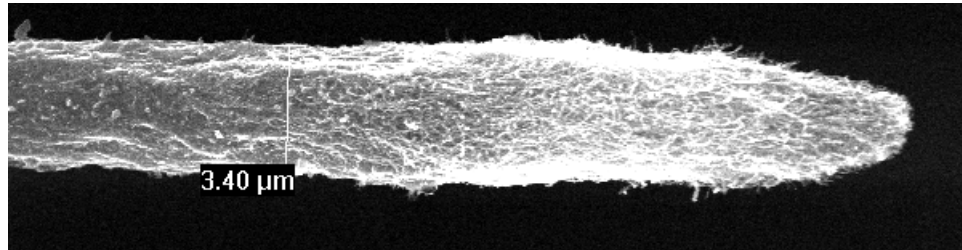


Figure 30: SEM images of a MWCNT probe with 100nm Parylene-C coating, the tip is exposed by the DC dielectric breakdown process.

We used FIB to have a sharper end which gives extensive control. An accelerated Gallium beam could successfully shave-off the probe. The final shape was similar to a sharp end of a flat bladed screwdriver, and Figure 31 shows the side view of the CNT probe after the FIB process. The Parylene-C coating survived the process except for the shaved edges (“>” shape ends, cutting planes are perpendicular to this page). The shaved surface was flat and no protruding CNTs could be found.

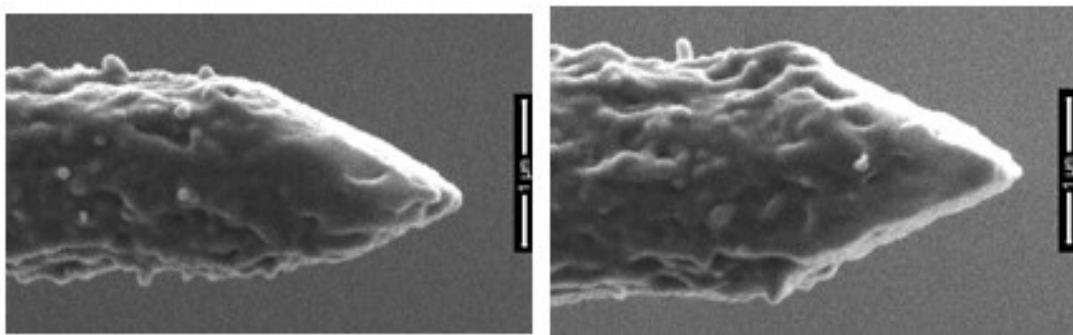


Figure 31: MWCNT probe tip end after coating Parylene-C and FIB process exposing CNT (the scale bar is 1 μm for both).

When diameter of probe near the tip is less than 2 μm , FIB shaped CNT probe could penetrate neurons.

3.3.2 Electrochemical characterization (CV and EIS)

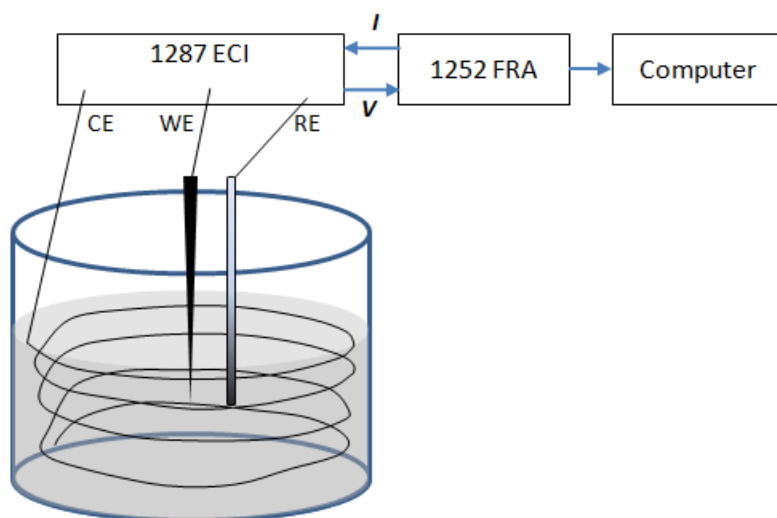


Figure 32: The three-electrode electrochemical cell setup for measuring electrical properties of MWCNT probe where CE (counter electrode), WE (working electrode), RE (reference electrode, Ag/AgCl pellet), ECI (electrochemical interface), FRA (frequency response analyzer). The setup is adapted from [65].

I used a three-electrode electrochemical cell with an impedance analyzer setup to understand electrical characteristics of MWCNT probes (The analyzer setup: Model # 1287 ECI (Electrochemical Interface), Model # 1252 FRA (Frequency Response Analyzer), Solatron Analytical, Hampshire, England). PBS (Phosphate buffered saline) solution

(0.25 M) is used to mimic the osmolarity of the brains of small animals. The measurement is performed at room temperature over the 1 Hz to 100 kHz range. With the setup shown in Figure 32, we did cyclic voltammetry (CV) and electrochemical impedance spectroscopy (EIS) of the CNT probes and conventional sharp recording with glass pipettes.

For CV, cyclic voltage (linearly varying between -1 and 1 V) is applied across the WE (working electrode, a CNT probe or a glass pipette) and the RE (reference electrode, Ag/AgCl pellet). The scan rates were 1,000 mV/sec and 100 mV/sec, and the results were not significantly different from each other. Considering that extracellular neuronal signals are in 1 kHz to 10 kHz range, and intracellular signals are much more diverse in frequency (10 kHz to less than 10 Hz), this measurement is not truly representative of the working condition. However, we can see there is not an oxidation-reduction (redox) reaction within the potential range (-1 to 1 V) from the simple hysteresis curves. This is good evidence that our CNT probe will be electrochemically stable with the working environment. It is also obvious that the CNT probe can store up and deliver significantly higher charge (energy) compared to the conventional glass pipette from the difference in enclosed area by the hysteresis.

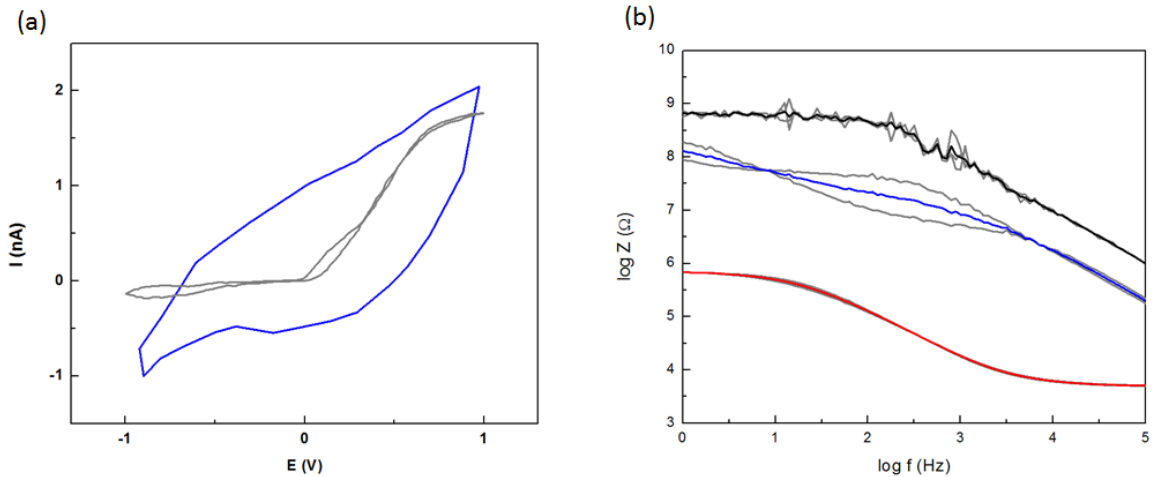


Figure 33: Electrochemical characterization of CNT probes. (a) Cyclic voltammetry (CV) for a glass electrode (grey) and a MWCNT probe with coating & FIB (blue), and (b) electrochemical impedance spectroscopy (EIS) result for sharp recording glass electrode (black, $n=3$), MWCNT probe without coating (red, $n=2$), and MWCNT probe with the coating and FIB process (blue, $n=2$).

As for the EIS measurement, the setup measures the potential difference between the MWCNT electrode and the Ag / AgCl pellet, while frequency controlled sinusoidal currents were supplied between the working electrode and the counter electrode with the 1287 ECI (input impedance 10 G Ω in parallel with 50 pF). To minimize effects of the series resistance, the reference electrode was positioned within 5 mm from the working electrode. Also, dipping depth of the CNT probe into the PBS solution was kept minimal. Compared to the conventional sharp recording glass electrodes, the CNT probe consistently showed one order lower $|Z|$ over the measured frequency range (1 to 100 kHz) as shown in Figure 33(b). Significant difference between blue and red lines is due

to successful insulation and controlled exposure, effectively reducing electrically active areas.

Combining the CV and EIS results, it is obvious that the capacitance component of the CNT probe is greater than that of glass electrodes. However, the resistive component of the CNT probe is significantly smaller enough to over-compensate the higher capacitance, and results in the lower $|Z|$ than the glass electrode overall. On an additional note, the impedance data trajectory on a complex Z plane ($-Z''$ ($-\text{Im}(Z)$) vs. Z' ($\text{Re}(Z)$)) of the CNT probe did not have a stereotypical shape, which can be modeled as an equivalent circuit with a few ideal electronic components [66].

As Zheng *et al.* described extensively [67], a classical simple interface model is not applicable for an ionic liquid and CNT electrode interface. In addition, our CNT probes have thin insulation and pores at different scales (micropores (diameter (d) < 2 nm), mesopores ($2 \text{ nm} < d < 50 \text{ nm}$), and macropores ($d > 50 \text{ nm}$)) which add more complexity [68]. When the CNT probe touches the PBS solution, the PBS solution wets near the tip area including not only the exposed CNTs surface but also the insulation coating. Therefore, any impedance measurement includes capacitance due to the insulation, and increasing the dipping depth amplifies the capacitive component in the measurement.

In related, but different work, Inaba *et al.* [69] observed a similar trend of impedance vs. frequency for their single-wall CNT (with a Parylene-C coating). They

explained the trend by stating that plateauing impedance at lower frequency range is due to dominating diffusion impedance for the lower range, while the effect at higher frequency range is largely due to capacitive impedance coming from the insulation.

Given complexity of the situation, further analysis of EIS data would require more sensitive measurement and comprehensive electrochemical study.

3.3.3 CNT probe as a surface scanning tip

For neuronal recording purposes, insulation and having a limited electrically active area is important. However, the morphology right after “pulling” out of the dielectrophoresis process is great for surface scanning tips – especially when only one CNT is sticking out at the end and the total length of the probe is less than 1 mm. Our MWCNT probes were able to be used as surface scanning tips with an AFM (atomic force microscope) setup, and were able to detect CNTs on a silicon surface.

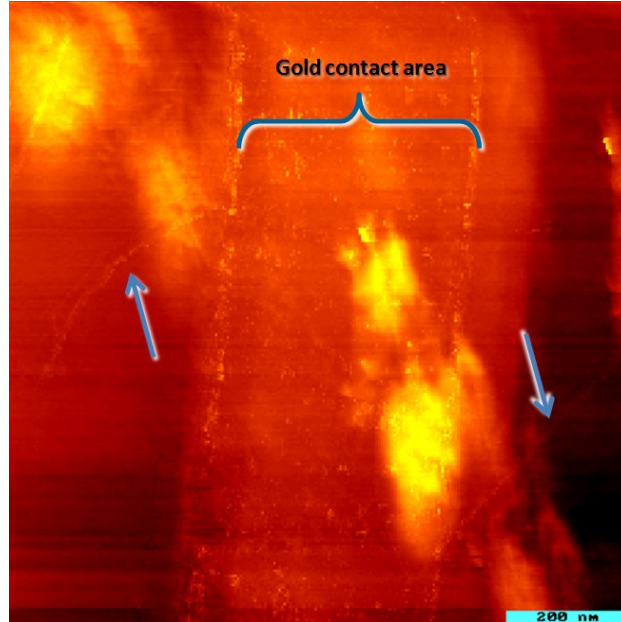


Figure 34: Nano scale surface profile scan data using a MWCNT probe as its scanning tip. Arrows are pointing toward two CNTs connected to a wide gold contact area on silicon substrate (The scale bar at lower right corner is 200 nm).

The most interesting observation of the AFM test was not achieving the nanotube resolution scanning. It was that the scan was done after the MWCNT probe had crashed the surface a few times. In a similar situation with conventional metal or silicon AFM or STM tips, the tips lose the necessary sharpness or break. Developing CNT probes for surface scanning was not a goal of the project, so there was not an extensive follow up experiment to further examine this. However, the physical resilience is obviously a major advantage especially for cryogenic or other harsh environmental measurements where swapping tips is not a simple task.

3.3.4 *In vitro* intracellular recording

3.3.4.1 Intracellular recording procedure

Subjects. Mice (*Mus musculus*, 34 days post natal, VGAT × C57) were used for the intracellular recordings, in accordance with a protocol approved by the Duke University Institutional Animal Care and Use Committee (A292-11-11).

Brain slices. After induction of inhalation anesthesia (Isoflurane), the mouse was decapitated, and the brain was removed rapidly and placed in oxygenated ice-cold Ca²⁺ free artificial CSF (ACSF). Coronal brain slices were cut at 400 μm thickness and transferred to a holding chamber (room temperature) for 2-4 h. Individual slices were transferred to an interface-type chamber (30 °C; medical Systems, Greenvale, NY) for intracellular recordings. The ACSF consisted of (in mM) 119 NaCl, 2.5 KCl, 1.3 MgCl₂, 2.5 CaCl₂, 1 NaH₂PO₄, 26.4 NaHCO₃, and 11 glucose, equilibrated with 95 % O₂ / 5 % CO₂.

Electrophysiological recordings. Before recording with a CNT probe, control sharp intracellular recordings were made with borosilicate glass pipettes (Sutter Instruments, Novato, CA) pulled to a final resistance of 80-150 MΩ when filled with 2M potassium acetate. Cell penetration was achieved by briefly “ringing” the electrode using

capacitance overcompensation, and the cell was then stabilized by passing regular hyperpolarizing current pulses through the recording electrode (-0.5 nA, 500 ms at 1Hz). Intracellular potentials were amplified with a headstage HS-2A X0.1LU and an Axoclamp 2B amplifier (Molecular Devices, Sunnyvale, CA) in bridge mode, low-pass filtered at 10 kHz, and digitized at 10 kHz. Targeted brain areas were the cortex layer II/III or V.

No filling solution was used with the CNT probe, but the rest of the recording setup was identical except the headstage HS-2A (X0.1LU) was used as a simple voltage follower to avoid the complexity that comes with the current injection. Therefore, there was no “ringing” involved for cell penetration with the CNT probe. To alternatively observe stimulated activity of the cell, independent electrical and optical stimulations were used. For an electrical stimulation, a concentric bipolar electrode (which looks like a blunt needle) was placed near the recording site on the brain slice, and injected positive or negative step function current (typically 10 μ A) briefly (1-10 ms). For the optical stimulation, an optical fiber was pointed directly above the recording site to deliver blue laser light (wavelength = 473 nm).

3.3.4.2 Intracellular recording with the CNT probe

Two conditions should be met to make intracellular recording successfully with CNT probes. First, the end diameter should be less than 2 μm , otherwise it fails to make decent seal after cell penetration. The other condition is compatibility of electrical characteristics of CNT probes with recording electronics (the headstage and Axoclamp 2B). The electronics are designed to compensate conventional glass pipette electrodes, therefore their resistance and capacitance compensation ranges were optimized for glass pipettes. We found that resistance compensation for the CNT probe is always lower than 1 $\text{M}\Omega$, and capacitance cannot be compensated properly with the electronics setup. Therefore, we use the headstage as a simple voltage follower, and adopted independent external stimulations. The intracellular recordings were recorded from cortical neurons in brain slices prepared from transgenic mice in which the light-activated ion channel channelrhodopsin 2 (ChR2) [70-72] was placed under the promoter for the vesicular glutamic acid transporter (VGAT), thus restricting expression of ChR2 to GABA-releasing inhibitory neurons. Focal illumination of the brain slice in the region of the recording site was then used to activate inhibitory synapses on an impaled cell, while a concentric bipolar stimulation electrode was placed adjacent to the recording site to electrically stimulate a population of neurons, which will drive a mixture of excitatory and inhibitory synaptic inputs. Using this approach, we were able to make intracellular recordings from a total of four cells using three different CNT probes, with a mean recording time of 3 minutes (198.1 ± 41.7 seconds, Fig. 35).

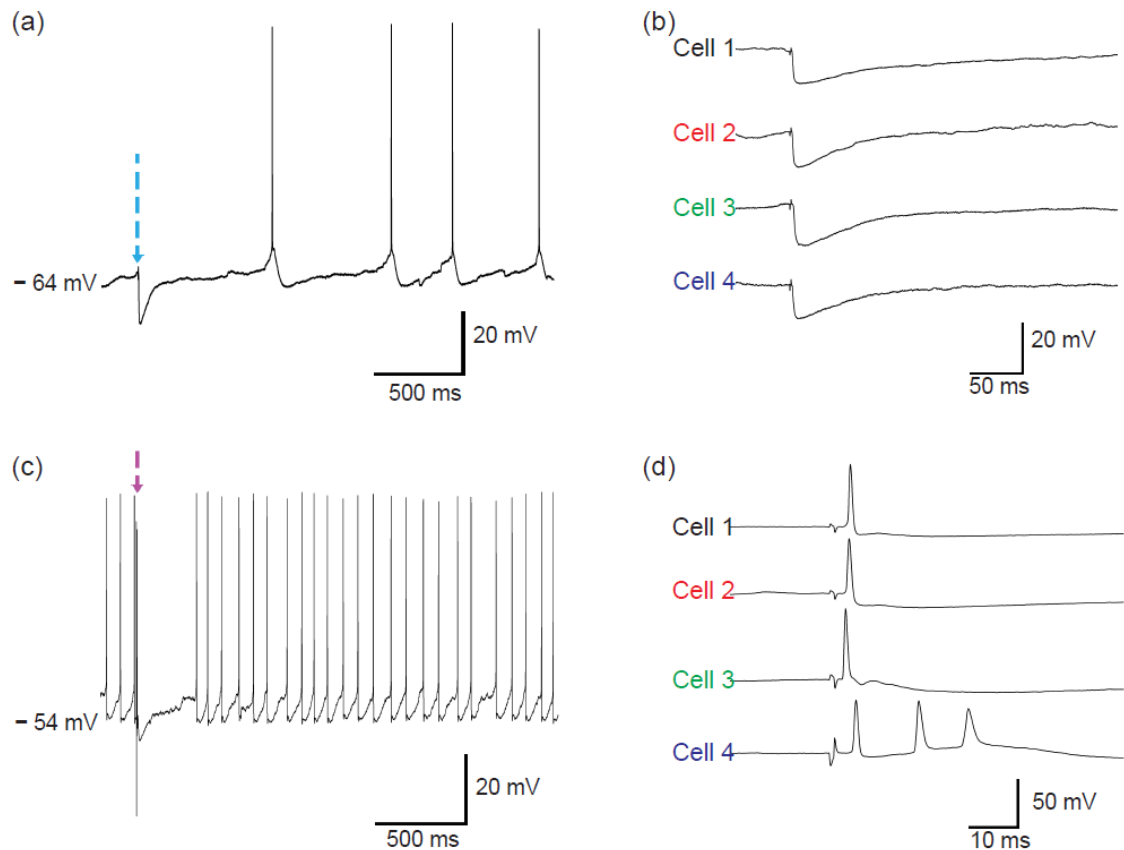


Figure 35: In vitro brain slice intracellular recording from mouse, cortical neurons. (a), Light-evoked inhibitory post synaptic potential (IPSP) recorded with a CNT probe from a neuron in a cortical brain slice prepared from a VGAT-CHR2 mouse. A brief light pulse was applied at the time marked by the arrow ($V_m = -64$ mV). (b), Expanded membrane potential records for CHR2 evoked IPSPs collected from four different cortical neurons. (c), Electrically-evoked EPSP from a cortical neuron in a mouse cortical brain slice ($V_m = -54$ mV). (d), Expanded membrane potential records of electrically-evoked EPSPs collected from four different cortical neurons.

Successful penetration was accompanied by a sharp drop in membrane potential (-57 ± 4.62 mV), and enabled the detection of spontaneous synaptic potentials and action

potentials (61.53 ± 7.92 mV). Focal illumination with 473 nm light pulses (2 ms) delivered via a 200 μ m (core diameter) micron fiber optic evoked short latency (4.94 ± 0.84 ms) hyperpolarizing membrane potential responses (11.86 ± 1.43 mV) in the impaled cell, consistent with ChR2-mediated activation of inhibitory inputs. Electrical stimulation evoked short latency depolarizing responses accompanied by action potentials or biphasic responses consisting of depolarizing and hyperpolarizing components, consistent with electrical activation of excitatory and inhibitory inputs. These observations indicate that the CNT probe developed here is suitable for intracellular recordings of membrane potential from cortical neurons.

3.3.5 *In vivo* extracellular recording

3.3.5.1 *In vivo* extracellular recording procedure

Subject. All Experiments were performed in accordance with the protocol approved by the Duke University Institutional Animal Care and Use Committee (A292-11-11). Male mice (*Mus musculus*, 30 days old) were anesthetized with ketamine (46 mg/kg) and xylazine (24 mg/kg) and supplemented with isoflurane (0.5-1.5 %) in oxygen. Core temperature of the mouse was monitored with a rectal probe (BAT-12, Physitemp Instruments, Clifton, NJ) and maintained at 36 ± 1 °C with a heating pad.

Surgery. A midline incision of the scalp was performed, and the skin was retracted. A small metal pin was attached to the cranium with dental cement, and the animal was fixed in a custom-made stereotaxic stage. A small craniotomy (~200 μm^2) was performed over the somatosensory cortex, and the dura overlying the brain was resected. The cortical surface was continuously kept moist.

Electrophysiological recordings. Before recording with the CNT probe, control extracellular recordings were made with a Carbostar-1 (Kation Scientific, Minneapolis, MN). The electrode was lowered into the brain 100 - 1,000 μm with a hydraulic micromanipulator (SD Instruments). Signals were amplified 1000 times and band pass filtered (100 Hz - 10 kHz) with a differential amplifier (A-M Systems, Sequim, WA) before being recorded with Spike 2 (Cambridge Electronic Design, Cambridge, England) at a sampling rate of 10 kHz.

3.3.5.2 *In vivo* extracellular recording with the CNT probe

We explored whether the CNT probe could be used to record neural activity in the somatosensory cortex of the anesthetized mouse ($n = 2$). When advanced into the cortex, all seven CNT probe samples were able to detect single and/or multi-unit

extracellular activity, in some cases revealing extremely large amplitude single unit events with a large signal to noise ratio ($S/N=9-34$, Fig. 36).

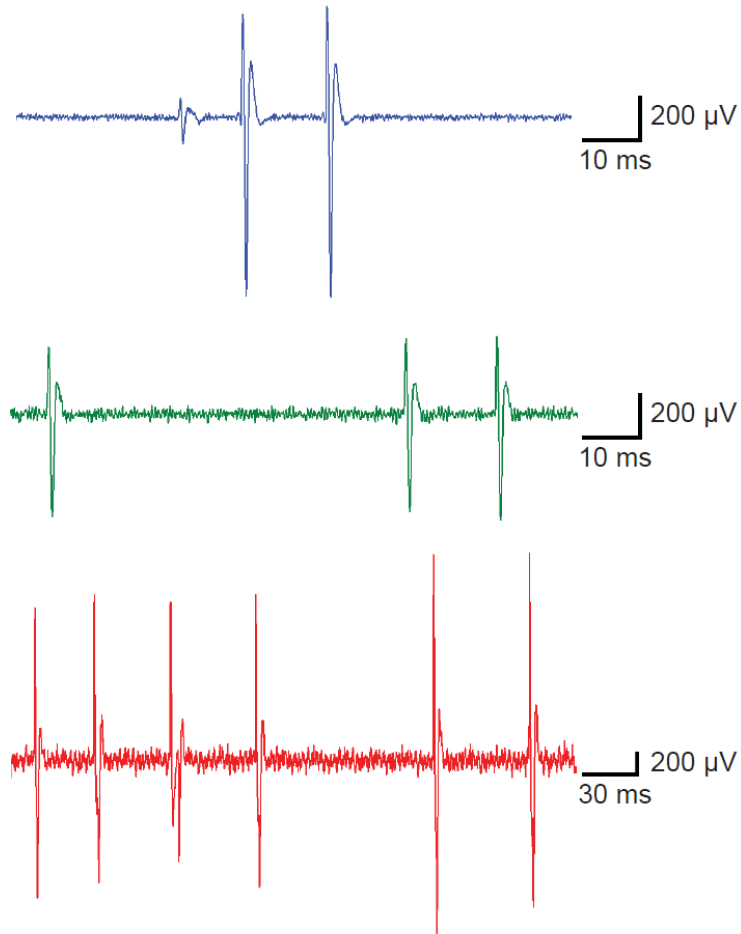


Figure 36: In vivo extracellular recordings from mouse brain somatosensory cortex. Three different extracellular recordings show well-isolated single unit activity.

Although intracellular recording configurations were not achieved in these preliminary experiments, the successful intracellular recordings made in brain slices

suggest that such recordings are feasible using CNT probes *in vivo*. An additional interesting observation was the elastic deformation of the CNT probes: when a small amount of off-axis force was applied to the CNT probes brain tissue, the shaft of the probe bent elastically without snapping. Because mechanical resilience of a neural electrode is crucial for *in vivo* intracellular recordings, the elastic feature of the CNT probe could offer advantages over conventional glass electrodes for such an application.

3.3.6 Future work

The advantages of CNT probes include relatively low impedance, mechanical flexibility, and bio-compatibility, suggesting that they may be suitable for a broad range of recording applications *in vivo* and *in vitro*. Full realization of this potential will require improving insulation layers, implementing capacitance compensation methods, and further refinement of the probe geometry.

Nonetheless, this study is proof that a pure CNT structure can be used as a neural recording electrode and is the first study to successfully do so.

4. Conclusions

We present technology innovations for intracellular neuronal recording from freely behaving small animals: a compact customized electronics and micro-drive system, and a CNT probe as a novel neuronal electrode.

The micro-drive system has been successfully used in awake and freely-behaving zebra finches and mice, and we have achieved recording greater than an hour from individual neurons on multiple occasions. The micro-drive system can be further customized for different and more complex tasks, such as an additional optical stimulation or a dual drive system for mice. These modifications can be done with little change on the headstage and the chassis of the micro motor. Close collaboration between a developer and an experimenter will be the key for better outcomes in this kind of development or customization.

The CNT probe can record intracellular and extracellular signals from both *in vitro* and *in vivo* settings. Even though further work is necessary for it to be used widely, this study is the first neural recording from vertebrate neurons using a pure carbon nanotube electrode. This study provides solid proof of concept and stepping stones toward application of carbon nanotubes in neurobiology and neural interfaces.

For future work, gaining more understanding of electrochemical characteristics of CNT probes will enable broader applications of them as a neural interface for

recording and stimulation. Along with the suggested chronic bio-compatibility, mechanical resilience against vibration and impact is a great feature of the CNT probes. And they will get broader attention if proper quantifications of those features are provided. On a different note, using CNT probes as a surface scanning tip was not a focus of this study as mentioned in section 3.3.3, but recovering from surface “crashing” is a great advantage over a metal or silicon based tip. Therefore, further characterization of CNT probes as a surface scanning tip could be very rewarding.

Appendix A. Anatomy of *in vivo* intracellular recording setup

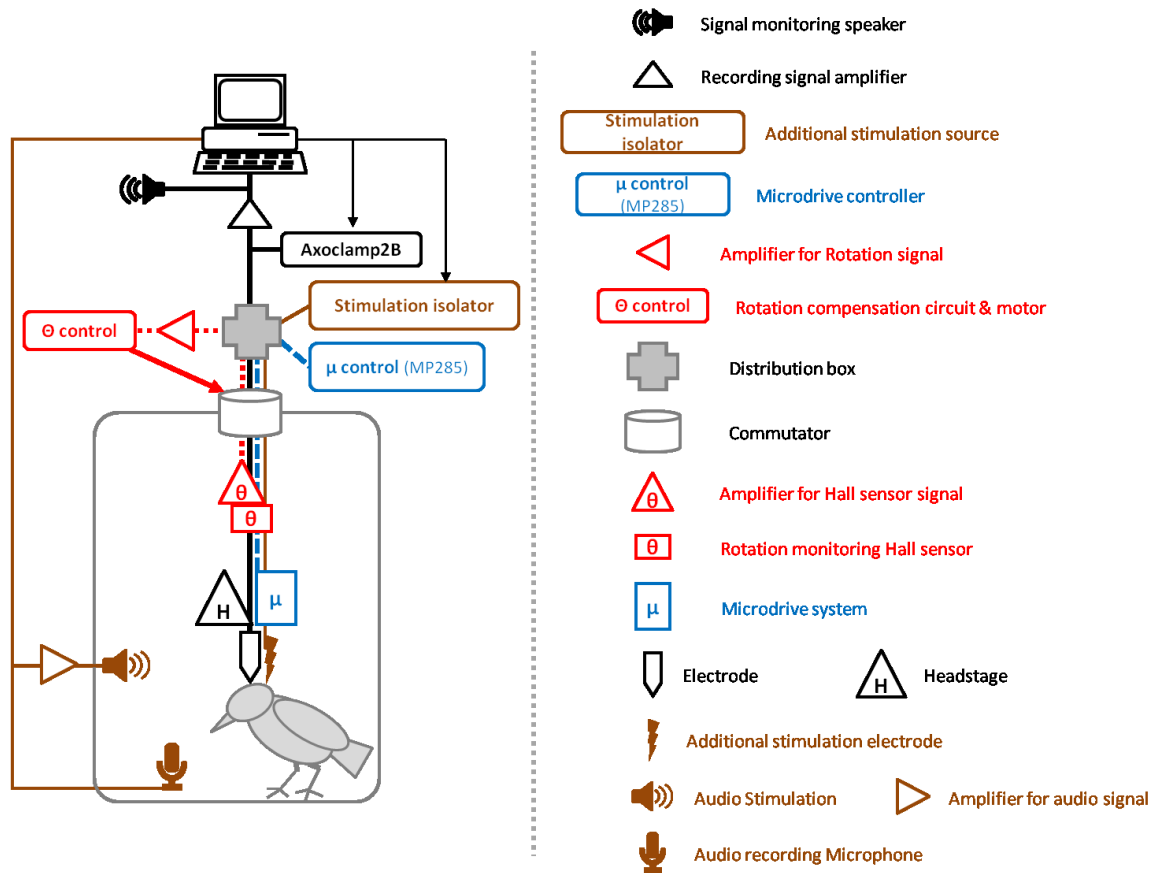


Figure 37: Components of *in vivo* intracellular recording setup.

- Commutator control related information can be found [10].
- Details of the mini-headstage are in Appendix B.
- Connection between the mini-headstage and the commutator and pin assignments are in Appendix C.
- Details of the distribution box are in Appendix D.

Appendix B. Mini-headstage PCB layout and its components

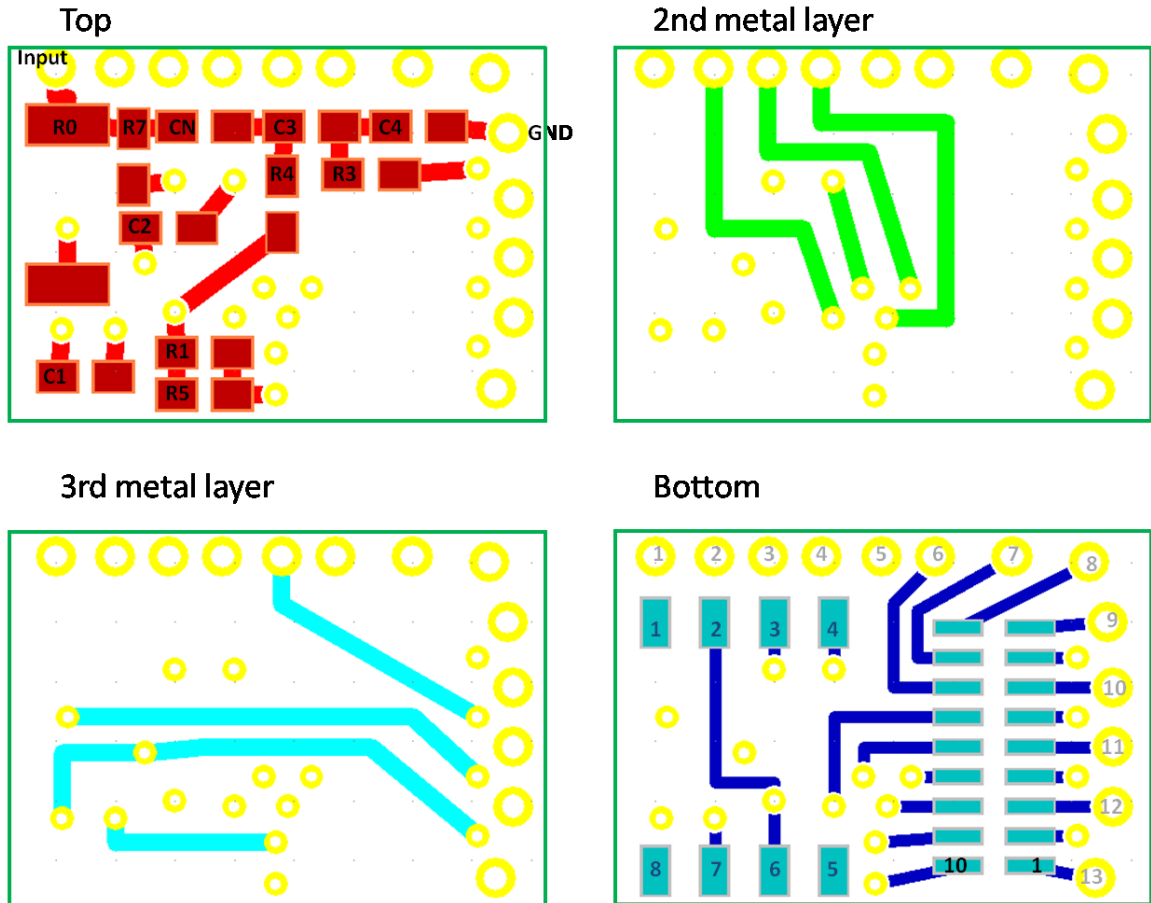


Figure 38: The mini-headstage PCB layout for each metal layer (projection views).

The mini-headstage is made with a FR4 PCB board (thickness 0.02", 10×15 mm) via Advanced Circuits (Aurora, CO. USA), and minimal trace and pitch of connecting lines on PCB was 0.007 and 0.0025 inches respectively.

The operational amplifier is a unity-gain precision FET opamp (OPA627AU-ND, Burr-Brown) and the connector has 18 positions Omnetics connector (P/N: A79008-001,

Type: NPD-18-AA-GS). Other components are listed in the Table 3. All the components are surface mount type, so a soldering paste and a toaster oven were used for the assembly. The top layer was assembled before the bottom layer, due to finer gaps between connector legs.

Table 3: Components of the mini-headstage.

Op-Amp	OPA627AU-ND
Connector	Omnetics18 positons male connector (P/N: A79008-001, Type: NPD-18-AA-GS)
R0	100 M Ω (100M)
R1	22.1 Ω (22R1)
R2	10 k Ω (10k0)
R3	221 Ω (221R)
R4	10 M Ω (10M)
R5	2.74 k Ω (2k74)
R7	4.75 k Ω , 1/8W (4k75)
C1	100 nF
C2	100 nF
C3	4,700 pF, 200V
C4	1 nF
CN	3.3 pF

Vias along the top and right side edges are numbered as shown in Figure 38, and the connections are assigned as shown in Table 4.

Table 4: Connection assignment on the mini-headstage.

Via number	Omnetics pin number		Via number
LC08	18	9	LV09 (GND)
LC07	17	8	VN
LC06	16	7	LC10
LC02	15	6	LC05
-VS	14	5	LC11
LC03	13	4	V0
LC04	12	3	LV12
+VS	11	2	OVS
VE	10	1	LC13

Appendix C. Connection between the mini-headstage and the commutator

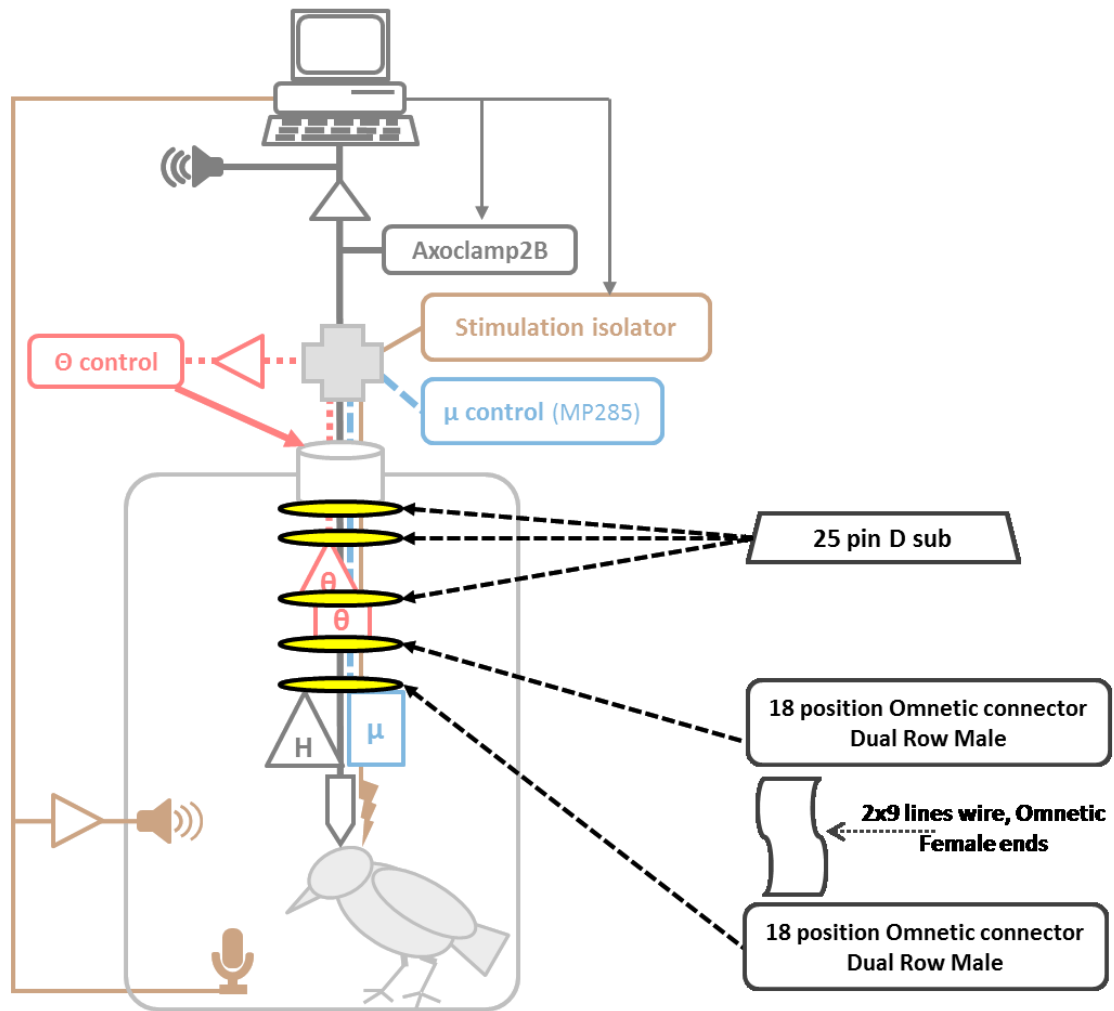


Figure 39: Components of *in vivo* intracellular recording setup.

As explained in Appendix B, the mini-headstage has the Omnetic connector with 18 channels. That is connected to the bottom of rotation monitoring hall sensor part by a 2x9 flexible line wire with a female end (P/N: A72098-001, Type: NSD-18-WD-18.0) and

the lines are braided with 3-strand braiding. After the braiding, the open end lines are manually soldered to another Omnetic connector (P/N: A79006-001, Type: NPD-18-DD-GS).

After the rotation monitoring hall sensor assembly, 25 pin D-sub connectors share the same connector assignment all the way up to the distribution box.

Table 5: Omnetics connectors and 25 pin D-sub connection assignments

Omnetics pin #	Function	D-sub 25 pin #	D-sub 25pin #	Function	AxoClamp	BNC out	MP-285
1	S2-	18	1	(E2-E3)x100			
2	OVS	4	2	Hall X10			
3	S2+	24	3	S1+		S1+	
4	V0	7	4	OVS	6		
5	S1-	6	5	E1+		E1+	
6	E3 (Pslc-)	11	6	S1-		S1-	
7	S1+	3	7	V0	14		
8	VN	10	8	E2+		E2+	
9	VGND	13	9	Mx			16
10	VE	16	10	VN	13		
11	+VS	19	11	E3+		E3+	
12	E2 (Pslc+)	8	12	My			20
13	My (PsV-)	12	13	VGND	8		
14	-VS	22	14	MGND			1
15	E1 (PsV+)	5	15	Mz			24
16	MGND	14	16	VE	11		
17	Mx	9	17			power +	
18	Mc	21	18	S2-		S2-	
	(E2-E3)x100	1	19	+VS	10		
	Hall output x 10	2	20			power -	
	Mz	15	21	MC			4
	+power supply	17	22	-VS	12		
	-power supply	20	23				
		23	24	S2+		S2+	
		25	25				

Appendix D. Distribution box

The distribution box connects the commutator (25 ch), the Axoclamp 2B (7/15 ch), two bipolar stimulations (2 BNCs), connections for rotation controls (5 ch + 2 power lines), TTL signal for relays (1 BNC), and the microdrive controller (MP-285+Fee control board, (7/25 ch). Therefore, 25 channels from the commutator get distributed as; $7 + 2 \times 2 + (5+2) + 7 = 25$ (TTL signal does not go to the comutator).

Housing of the box is custom made out of an aluminum chassis (8×4×1”), and all the connections inside of the box are made on a solderless breadboard (22 AWG, 126 ch with 4 bus strips). The breadboard is partitioned into 4 groups; the commutator (1-13), the Axoclamp 2B (14-21), relay switches (25-31, 34-40, 43-49), and the MP-285 (51-63).

Each group’s name represents where the connection goes to, except the relay switches which alternating ground and motor signal (M_x, M_y, M_z) on commend from MP-285 (TTL signal). This part disconnects the motor signals during non-operation time, which prevents sinusoidal noise contamination on the recording signal. The relays are RHEED switches (12V, 500 Ω , 288 mW) which require separate amplification of the original TTL signal before the signal gets distributed among three relays. Connections between groups are manually made with electrical connection wires. (For examples, commu13 (1Left) is connected to axo8 (14L) for V_{GND} , and mp16 (61Right) is connected to 40R – 34R (via the relay) then to commu9 (5L) for M_x .

Additionally, there are resistor networks which serve as micro-motor protection (preventing undesired current surge from MP-285) in a situation where not all three motors are connected. In other words, when only one micro-motor (M_x) is connected, two resistor networks are installed. Each resistor is matching resistive character between two terminals of used micro-motor, and we used $7.5 \Omega / 0.25 \text{ W}$ resistors for the resistor networks.

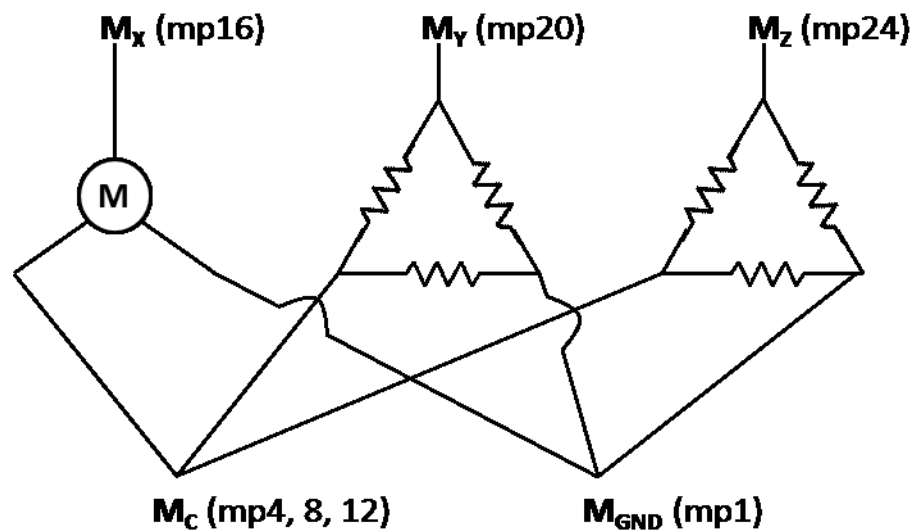


Figure 40: The resistor networks with on motor (M_x) for current surge protection. The mp## are the terminal numbers on the breadboard.

Table 6: The distribution box (breadboard) connections.

Function	Numbers on the breadboard			Function
VGND	commu13	1	commu25	
My	commu12	2	commu24	S2+
E3 (Pslc-)	commu11	3	commu23	
VN	commu10	4	commu22	-VS
Mx	commu9	5	commu21	Mc
E2 (Pslc+)	commu8	6	commu20	-power supply
V0	commu7	7	commu19	+VS
S1-	commu6	8	commu18	S2-
E1 (PsV+)	commu5	9	commu17	+power supply
OVS	commu4	10	commu16	VE
S1+	commu3	11	commu15	Mz
Hall output x 10 (E2-E3)x100	commu2	12	commu14	MGND
VGND	commu1	13		
	axo8	14	axo15	
	axo7	15	axo14	V0
OVS	axo6	16	axo13	VN
	axo5	17	axo12	-VS
	axo4	18	axo11	VE
	axo3	19	axo10	+VS
	axo2	20	axo9	
	axo1	21		
		22		
		23		
		24		
	R1	25	R14	
TTL-	R2	26		
		27		
		28		
		29		
TTL+	R6	30		
	R7	31	R8	MP-Mz
		32		
		33		
	R1	34	R14	
TTL-	R2	35		
		36		
		37		
		38		
TTL+	R6	39		
MP-My	R7	40	R8	MP-Mx
		41		
		42		
MP-Mc	R1	43	R14	
TTL-	R2	44		
		45		
		46		
		47		
TTL+	R6	48		
	R7	49	R8	MP-MGND
		50		
	mp13	51		
Mc	mp12	52	mp25	
	mp11	53	mp24	Mz
	mp10	54	mp23	
	mp9	55	mp22	
Mc	mp8	56	mp21	
	mp7	57	mp20	My
	mp6	58	mp19	
	mp5	59	mp18	
Mc	mp4	60	mp17	
	mp3	61	mp16	Mx
	mp2	62	mp15	
MGND	mp1	63	mp14	

References

- [1] D. Purves, *Neuroscience*. Sunderland, Mass.: Sinauer Associates, Publishers, 2004.
- [2] S. Herculano-Houzel, "The human brain in numbers: a linearly scaled-up primate brain," *Frontiers in Human Neuroscience*, vol. 3, 2009-November-9 2009.
- [3] R. W. Williams, "Mapping genes that modulate mouse brain development: a quantitative genetic approach," *Results and problems in cell differentiation*, vol. 30, pp. 21-49, 2000.
- [4] H. Jia, N. L. Rochefort, X. Chen, and A. Konnerth, "Dendritic organization of sensory input to cortical neurons in vivo," *Nature*, vol. 464, pp. 1307-12, Apr 29 2010.
- [5] Y. Jeantet and Y. H. Cho, "Design of a twin tetrode microdrive and headstage for hippocampal single unit recordings in behaving mice," *J Neurosci Methods*, vol. 129, pp. 129-34, Oct 30 2003.
- [6] T. Sato, T. Suzuki, and K. Mabuchi, "Independent hydraulic positioning for an implantable multi-electrode array," in *3rd International IEEE EMBS Conference on Neural Engineering, May 2, 2007 - May 5, 2007*, Kohala Coast, HI, United states, 2007, pp. 73-76.
- [7] J. Yamamoto and M. A. Wilson, "Large-scale chronically implantable precision motorized microdrive array for freely behaving animals," *J Neurophysiol*, vol. 100, pp. 2430-40, Oct 2008.
- [8] S. Yang, S. Lee, K. Park, H. Jeon, Y. Huh, J. Cho, *et al.*, "Piezo motor based microdrive for neural signal recording," in *30th Annual International Conference of the IEEE Engineering in Medicine and Biology Society, EMBS'08, August 20, 2008 - August 25, 2008*, Vancouver, BC, Canada, 2008, pp. 3364-3367.
- [9] S. Yang, S. Lee, K. Park, J. Kim, J. Cho, H.-S. Shin, *et al.*, "Highly-accurate, implantable micromanipulator for single neuron recordings," in *2010 IEEE International Conference on Robotics and Automation, ICRA 2010, May 3, 2010 - May 7, 2010*, Anchorage, AK, United states, 2010, pp. 5070-5075.

- [10] M. S. Fee and A. Leonardo, "Miniature motorized microdrive and commutator system for chronic neural recording in small animals," *J Neurosci Methods*, vol. 112, pp. 83-94, Dec 15 2001.
- [11] L. Giacchino and Y. C. Tai, "Electrolysis-based parylene-balloon actuators," in *TRANSDUCERS 2009 - 15th International Conference on Solid-State Sensors, Actuators and Microsystems, June 21, 2009 - June 25, 2009, Denver, CO, United states, 2009*, pp. 2397-2400.
- [12] N. Jackson, A. Sridharan, S. Anand, M. Baker, M. Okandan, and J. Muthuswamy, "Long-Term Neural Recordings Using MEMS Based Movable Microelectrodes in the Brain," *Front Neuroeng*, vol. 3, p. 10, 2010 Jun 2010.
- [13] S. Anand, J. Sutanto, M. S. Baker, M. Okandan, and J. Muthuswamy, "Electrothermal Microactuators With Peg Drive Improve Performance for Brain Implant Applications," *Journal of Microelectromechanical Systems*, vol. 21, pp. 1172-1186, Oct 2012.
- [14] S. Park, E. Yoon, S. Lee, H. S. Shin, H. Park, B. Kim, *et al.*, "The development of a PZT-based microdrive for neural signal recording," *Smart Materials & Structures*, vol. 17, Apr 2008.
- [15] A. J. Doupe and P. K. Kuhl, "Birdsong and human speech: common themes and mechanisms," *Annu Rev Neurosci*, vol. 22, pp. 567-631, 1999.
- [16] M. A. Long, D. Z. Jin, and M. S. Fee, "Support for a synaptic chain model of neuronal sequence generation," *Nature*, vol. 468, pp. 394-9, Nov 18 2010.
- [17] S. V. N. T. Kuchibhatla, A. S. Karakoti, D. Bera, and S. Seal, "One dimensional nanostructured materials," *Progress in Materials Science*, vol. 52, pp. 699-913, Jul 2007.
- [18] M. S. Dresselhaus, G. Dresselhaus, and P. Avouris, *Carbon nanotubes : synthesis, structure, properties, and applications*. Berlin; New York: Springer, 2001.
- [19] A. V. Melechko, V. I. Merkulov, T. E. McKnight, M. A. Guillorn, K. L. Klein, D. H. Lowndes, *et al.*, "Vertically aligned carbon nanofibers and related structures: Controlled synthesis and directed assembly," *Journal of Applied Physics*, vol. 97, pp. 041301-39, Feb 15 2005.

- [20] E. W. Keefer, B. R. Botterman, M. I. Romero, A. F. Rossi, and G. W. Gross, "Carbon nanotube coating improves neuronal recordings," *Nat Nanotechnol*, vol. 3, pp. 434-9, Jul 2008.
- [21] E. D. de Asis, Jr., J. Leung, S. Wood, and C. V. Nguyen, "Empirical study of unipolar and bipolar configurations using high resolution single multi-walled carbon nanotube electrodes for electrophysiological probing of electrically excitable cells," *Nanotechnology*, vol. 21, p. 125101, Mar 26 2010.
- [22] S. R. Yeh, Y. C. Chen, H. C. Su, T. R. Yew, H. H. Kao, Y. T. Lee, *et al.*, "Interfacing Neurons both Extracellularly and Intracellularly Using Carbon - Nanotube Probes with Long-Term Endurance," *Langmuir*, vol. 25, pp. 7718-7724, Jul 7 2009.
- [23] C. D. Harvey, F. Collman, D. A. Dombeck, and D. W. Tank, "Intracellular dynamics of hippocampal place cells during virtual navigation," *Nature*, vol. 461, pp. 941-6, Oct 15 2009.
- [24] A. K. Lee, I. D. Manns, B. Sakmann, and M. Brecht, "Whole-cell recordings in freely moving rats," *Neuron*, vol. 51, pp. 399-407, Aug 17 2006.
- [25] J. Epsztein, M. Brecht, and A. K. Lee, "Intracellular determinants of hippocampal CA1 place and silent cell activity in a novel environment," *Neuron*, vol. 70, pp. 109-20, Apr 14 2011.
- [26] J. F. Prather, S. Peters, S. Nowicki, and R. Mooney, "Precise auditory-vocal mirroring in neurons for learned vocal communication," *Nature*, vol. 451, pp. 305-10, Jan 17 2008.
- [27] S. K. Arfin, M. A. Long, M. S. Fee, and R. Sarpeshkar, "Wireless neural stimulation in freely behaving small animals," *J Neurophysiol*, vol. 102, pp. 598-605, Jul 2009.
- [28] R. A. Blum, "An electronic system for extracellular neural stimulation and recording," Ph.D. 3271476, Georgia Institute of Technology, United States -- Georgia, 2007.
- [29] D. P. Nguyen, S. P. Layton, G. Hale, S. N. Gomperts, T. J. Davidson, F. Kloosterman, *et al.*, "Micro-drive array for chronic in vivo recording: tetrode assembly," *J Vis Exp*, p. e1098, 2009.

- [30] S. J. Thomas, R. R. Harrison, A. Leonardo, and M. S. Reynolds, "A battery-free multi-channel digital neural/EMG telemetry system for flying insects," in *Biomedical Circuits and Systems Conference (BioCAS), 2011 IEEE*, 2011, pp. 229-232.
- [31] J. Morizio, P. Irazoqui, V. Go, and J. Parmentier, "Wireless headstage for neural prosthetics," in *2nd International IEEE EMBS Conference on Neural Engineering, 2005, March 16, 2005 - March 19, 2005*, Arlington, VA, United states, 2005, pp. 414-417.
- [32] N. Jackson, S. Anand, M. Okandan, and J. Muthuswamy, "Nonhermetic Encapsulation Materials for MEMS-Based Movable Microelectrodes for Long-Term Implantation in the Brain," *J Microelectromech Syst*, vol. 18, pp. 1234-1245, Jan 1 2009.
- [33] A. Instruments, *The Axon guide for electrophysiology & biophysics : laboratory techniques*. Foster City, CA: Axon Instruments, Inc., 1993.
- [34] H. J. Bischof, "A stereotaxic headholder for small birds," *Brain Res Bull*, vol. 7, pp. 435-6, Oct 1981.
- [35] E. D. Jarvis, O. Gunturkun, L. Bruce, A. Csillag, H. Karten, W. Kuenzel, *et al.*, "Avian brains and a new understanding of vertebrate brain evolution," *Nat Rev Neurosci*, vol. 6, pp. 151-9, Feb 2005.
- [36] K. T. Brown and D. G. Flaming, *Advanced micropipette techniques for cell physiology*. Chichester West Sussex ; New York: Wiley, 1986.
- [37] N. A. Blum, B. G. Carkhuff, H. K. Charles, Jr., R. L. Edwards, and R. A. Meyer, "Multisite microprobes for neural recordings," *IEEE Trans Biomed Eng*, vol. 38, pp. 68-74, Jan 1991.
- [38] G. Ensell, D. J. Banks, D. J. Ewins, W. Balachandran, and P. R. Richards, "Silicon based microelectrodes for neurophysiology fabricated using a gold metallization nitride passivation system," *Journal of Microelectromechanical Systems*, vol. 5, pp. 117-121, Jun 1996.
- [39] L. A. Geddes, *Principles of applied biomedical instrumentation*: New York, Wiley, 1968.
- [40] L. A. Geddes, *Electrodes and the measurement of bioelectric events*: New York, Wiley-Interscience, 1972.

- [41] D. T. Kewley, M. D. Hills, D. A. Borkholder, I. E. Opris, N. I. Maluf, C. W. Storment, *et al.*, "Plasma-etched neural probes," *Sensors and Actuators a-Physical*, vol. 58, pp. 27-35, Jan 1997.
- [42] B. W. Kristensen, J. Noraberg, P. Thiebaud, M. Koudelka-Hep, and J. Zimmer, "Biocompatibility of silicon-based arrays of electrodes coupled to organotypic hippocampal brain slice cultures," *Brain Res*, vol. 896, pp. 1-17, Mar 30 2001.
- [43] W. L. C. Rutten, H. J. Vanwier, and J. H. M. Put, "Sensitivity and Selectivity of Intraneural Stimulation Using a Silicon Electrode Array," *IEEE Transactions on Biomedical Engineering*, vol. 38, pp. 192-198, Feb 1991.
- [44] K. Najafi, "Solid-State Microsensors for Cortical Nerve Recordings," *Ieee Engineering in Medicine and Biology Magazine*, vol. 13, pp. 375-387, Jun-Jul 1994.
- [45] M. HajjHassan, V. Chodavarapu, and S. Musallam, "NeuroMEMS: Neural Probe Microtechnologies," *Sensors*, vol. 8, pp. 6704-6726, Oct 2008.
- [46] M. R. Angle and A. T. Schaefer, "Neuronal recordings with solid-conductor intracellular nanoelectrodes (SCINeS)," *PLoS One*, vol. 7, p. e43194, 2012.
- [47] S. Musallam, M. J. Bak, P. R. Troyk, and R. A. Andersen, "A floating metal microelectrode array for chronic implantation," *J Neurosci Methods*, vol. 160, pp. 122-7, Feb 15 2007.
- [48] X. Duan, R. Gao, P. Xie, T. Cohen-Karni, Q. Qing, H. S. Choe, *et al.*, "Intracellular recordings of action potentials by an extracellular nanoscale field-effect transistor," *Nat Nanotechnol*, vol. 7, pp. 174-9, Mar 2012.
- [49] J. T. Robinson, M. Jorgolli, A. K. Shalek, M. H. Yoon, R. S. Gertner, and H. Park, "Vertical nanowire electrode arrays as a scalable platform for intracellular interfacing to neuronal circuits," *Nat Nanotechnol*, vol. 7, pp. 180-4, Mar 2012.
- [50] R. A. Normann, E. M. Maynard, P. J. Rousche, and D. J. Warren, "A neural interface for a cortical vision prosthesis," *Vision Res*, vol. 39, pp. 2577-87, Jul 1999.
- [51] K. D. Wise, D. J. Anderson, J. F. Hetke, D. R. Kipke, and K. Najafi, "Wireless implantable microsystems: High-density electronic interfaces to the nervous system," in *Biomedical Applications for Mems and Microfluidics*, 2004, pp. 76-97.

- [52] T. Gabay, E. Jakobs, E. Ben-Jacob, and Y. Hanein, "Engineered self-organization of neural networks using carbon nanotube clusters," *Physica a-Statistical Mechanics and Its Applications*, vol. 350, pp. 611-621, May 15 2005.
- [53] H. Hui, N. Yingchun, V. Montana, R. C. Haddon, and V. Parpura, "Chemically functionalized carbon nanotubes as substrates for neuronal growth," *Nano Letters*, vol. 4, pp. 507-11, 2004.
- [54] V. Lovat, D. Pantarotto, L. Lagostena, B. Cacciari, M. Grandolfo, M. Righi, *et al.*, "Carbon nanotube substrates boost neuronal electrical signaling," *Nano Lett*, vol. 5, pp. 1107-10, Jun 2005.
- [55] M. P. Mattson, R. C. Haddon, and A. M. Rao, "Molecular functionalization of carbon nanotubes and use as substrates for neuronal growth," *Journal of Molecular Neuroscience*, vol. 14, pp. 175-182, Jun 2000.
- [56] K. Matsumoto, C. Sato, Y. Naka, A. Kitazawa, R. L. Whitby, and N. Shimizu, "Neurite outgrowths of neurons with neurotrophin-coated carbon nanotubes," *J Biosci Bioeng*, vol. 103, pp. 216-20, Mar 2007.
- [57] E. D. de Asis Jr, J. Leung, S. Wood, and C. V. Nguyen, "High spatial resolution single multiwalled carbon nanotube electrode for stimulation, recording, and whole cell voltage clamping of electrically active cells," *Applied Physics Letters*, vol. 95, 2009.
- [58] M. G. Schrlau and H. H. Bau, "Carbon-based nanoprobes for cell biology," *Microfluidics and Nanofluidics*, vol. 7, pp. 439-450, Oct 2009.
- [59] M. G. Schrlau, E. M. Falls, B. L. Ziober, and H. H. Bau, "Carbon nanopipettes for cell probes and intracellular injection," *Nanotechnology*, vol. 19, p. 015101, Jan 9 2008.
- [60] N. A. Kouklin, W. E. Kim, A. D. Lazareck, and J. M. Xu, "Carbon nanotube probes for single-cell experimentation and assays," *Applied Physics Letters*, vol. 87, pp. 1-3, Oct 24 2005.
- [61] J. Ma, J. Tang, H. Zhang, N. Shinya, and L. C. Qin, "Ultrathin carbon nanotube fibrils of high electrochemical capacitance," *ACS Nano*, vol. 3, pp. 3679-83, Nov 24 2009.

- [62] J. Tang, B. Gao, H. Geng, O. D. Velev, L.-C. Qin, and O. Zhou, "Assembly of 1D Nanostructures into Sub-micrometer Diameter Fibrils with Controlled and Variable Length by Dielectrophoresis," *Advanced Materials*, vol. 15, pp. 1352-1355, 2003.
- [63] L. Ottaviano, L. Lozzi, and S. Santucci, "Scanning Auger microscopy study of W tips for scanning tunneling microscopy," *Review of Scientific Instruments*, vol. 74, pp. 3368-3378, Jul 2003.
- [64] E. M. Schmidt, J. S. McIntosh, and M. J. Bak, "Long-term implants of Parylene-C coated microelectrodes," *Med Biol Eng Comput*, vol. 26, pp. 96-101, Jan 1988.
- [65] X. F. Wei and W. M. Grill, "Impedance characteristics of deep brain stimulation electrodes in vitro and in vivo," *J Neural Eng*, vol. 6, p. 046008, Aug 2009.
- [66] B. E. Conway, *Electrochemical supercapacitors : scientific fundamentals and technological applications*. New York: Plenum Press, pp. 554-555, 1999.
- [67] J. P. Zheng, P. C. Goonetilleke, C. M. Pettit, and D. Roy, "Probing the electrochemical double layer of an ionic liquid using voltammetry and impedance spectroscopy: A comparative study of carbon nanotube and glassy carbon electrodes in [EMIM]+[EtSO₄]-," *Talanta*, vol. 81, pp. 1045-1055, 5/15/ 2010.
- [68] A. G. Pandolfo and A. F. Hollenkamp, "Carbon properties and their role in supercapacitors," *Journal of Power Sources*, vol. 157, pp. 11-27, 6/19/ 2006.
- [69] A. Inaba, Y. Takei, T. Kan, K. Matsumoto, and I. Shimoyama, "Electrochemical impedance measurement of a carbon nanotube probe electrode," *Nanotechnology*, vol. 23, p. 485302, 2012.
- [70] E. S. Boyden, F. Zhang, E. Bamberg, G. Nagel, and K. Deisseroth, "Millisecond-timescale, genetically targeted optical control of neural activity," *Nat Neurosci*, vol. 8, pp. 1263-8, Sep 2005.
- [71] G. Nagel, M. Brauner, J. F. Liewald, N. Adeishvili, E. Bamberg, and A. Gottschalk, "Light activation of channelrhodopsin-2 in excitable cells of *Caenorhabditis elegans* triggers rapid behavioral responses," *Curr Biol*, vol. 15, pp. 2279-84, Dec 20 2005.

- [72] G. Nagel, T. Szellas, W. Huhn, S. Kateriya, N. Adeishvili, P. Berthold, *et al.*, "Channelrhodopsin-2, a directly light-gated cation-selective membrane channel," *Proc Natl Acad Sci U S A*, vol. 100, pp. 13940-5, Nov 25 2003.

Biography

Inho Yoon was born in Incheon, South Korea, on November 30, 1974. He received his Bachelor of Engineering Degree and the first Master of Science Degree in Material Science & Engineering from Korea University, Seoul, South Korea, in 1999, and 2001 respectively. He received his second Master of Science Degree in Mechanical Engineering from Georgia Institute of Technology, Atlanta, GA USA, in 2005. He joined the doctoral program in the Department of Electrical and Computer Engineering, Duke University, Durham, NC in 2006, where he also completed a Master of Engineering Management Program, in 2010.

Journal Publications

- [1] I. Yoon, K. Hamaguchi, I. V. Borzenets, G. Finkelstein, R. Mooney, and B. R. Donald, "Intracellular neural recording with pure carbon nanotube probes," (submitted to a journal), 2013.
- [2] K. Hamaguchi, K. A. Tschida, I. Yoon, B. R. Donald, and R. Mooney, "Mechanisms underlying a synaptic trace of auditory feedback in a sensorimotor nucleus important to learned birdsong," (submitted to a journal), 2013.
- [3] T.-H. Kim, M. Losurdo, S. Choi, I. Yoon, G. Bruno, and A. Brown, "Real-time studies of In-adlayer during PAMBE of InGaN/GaN MQWs," *physica status solidi C*, vol. 9, pp. 1036-1039, 2012.
- [4] I. V. Borzenets, I. Yoon, M. M. Prior, B. R. Donald, R. D. Mooney, and G. Finkelstein, "Ultra-sharp metal and nanotube-based probes for applications in scanning microscopy and neural recording," *Journal of Applied Physics*, vol. 111, 2012.

- [5] I. Yoon, C. Yi, T. Kim, A. S. Brown, and A. Seabaugh, "Effect of surface pretreatment and substrate orientation on the characteristics of InAs quantum dots on Si and SiO₂ substrates," *Journal of Vacuum Science & Technology B: Microelectronics and Nanometer Structures*, vol. 25, pp. 945-947, 2007.
- [6] A. Osorno, S. Tereshko, I. Yoon, and S. Danyluk, "Dynamics of the Formation of the Subambient Pressure Distribution During Chemical-Mechanical Polishing," *ASME Conference Proceedings*, vol. 2007, pp. 1081-1082, 2007.
- [7] W. Bin, D. Wheeler, Y. Changhyun, I. Yoon, S. Jha, A. Brown, et al., "InAs growth on submicron (100) SOI islands for InAs-Si composite channel MOSFETs," in *Semiconductor Device Research Symposium, 2007 International*, pp. 381-382, 2007.
- [8] S. H. Ng, C. F. Higgs III, I. Yoon, and S. Danyluk, "An Analysis of Mixed Lubrication in Chemical Mechanical Polishing," *Journal of Tribology*, vol. 127, pp. 287-292, 2005.
- [9] S. H. Ng, L. Borucki, C. F. Higgs, I. Yoon, A. Osorno, and S. Danyluk, "Tilt and Interfacial Fluid Pressure Measurements of a Disk Sliding on a Polymeric Pad," *Journal of Tribology*, vol. 127, pp. 198-205, 2005.
- [10] C. F. Higgs, S. H. Ng, L. Borucki, I. Yoon, and S. Danyluk, "A Mixed-Lubrication Approach to Predicting CMP Fluid Pressure Modeling and Experiments," *Journal of The Electrochemical Society*, vol. 152, pp. G193-G198, 2005.
- [11] S. H. Ng, I. Yoon, C. F. Higgs, and S. Danyluk "Wafer-Bending Measurements in CMP," *Journal of The Electrochemical Society*, vol. 151, pp. G819-G823, 2004.
- [12] S. H. Ng, C. M. Zettner, C. Zhou, I. Yoon, S. Danyluk, M. Sacks, et al., "Nanoparticulate and Interfacial Mechanics in Confined Geometries Typical of Chemical-Mechanical Planarization," *ASME Conference Proceedings*, vol. 2003, pp. 199-206, 2003.
- [13] S. H. Ng, R. Hight, C. Zhou, I. Yoon, and S. Danyluk, "Pad Soaking Effect on Interfacial Fluid Pressure Measurements During CMP," *Journal of Tribology*, vol. 125, pp. 582-586, 2003.

- [14] C. F. Higgs, S. H. Ng, I. Yoon, L. Shan, L. Yap, and S. Danyluk, "Mechanical Modeling of the 2D Interfacial Slurry Pressure in CMP," MRS Online Proceedings Library, vol. 767, pp. null-null, 2003.
- [15] I. Yoon, S. H. Ng, R. Hight, C. Zhou, C. F. I. Higgs , L. Yao, et al., "Dishing and Erosion in Chemical Mechanical Polishing of Electroplated Copper " Asia Tribology, 2002.
- [16] D. Lim, I. Yoon, and S. Danyluk, "Effect of electric field on chemical mechanical polishing of langasite," Wear, vol. 249, pp. 397-400, 2001.